MICROCOPY RESOLUTION TEST CHART

NATIONAL BUREAU OF STANDARDS-1963

NAVAL POSTGRADUATE SCHOOL
Monterey, California

THESIS

AN EXAMINATION OF TURBULENT DISSIPATION

IN THE MARINE BOUNDARY LAYER

by

George William Karch

December 1976

Thesis Advisor: K. L. Davidson

REPORT DOCUMENTATION PAGE

**READ INSTRUCTIONS
BEFORE COMPLETING FORM**

1. REPORT NUMBER	2. GOVT ACCESSION NO.	3. RECIPIENT'S CATALOG NUMBER

4. TITLE (and Subtitle)

An Examination of Turbulent Dissipation in the Marine Boundary Layer.

5. TYPE OF REPORT & PERIOD COVERED

Master's Thesis

6. PERFORMING ORG. REPORT NUMBER

7. AUTHOR(s)

George William Karch

8. CONTRACT OR GRANT NUMBER(s)

9. PERFORMING ORGANIZATION NAME AND ADDRESS

Naval Postgraduate School
Monterey, California 93940

10. PROGRAM ELEMENT, PROJECT, TASK AREA & WORK UNIT NUMBERS

11. CONTROLLING OFFICE NAME AND ADDRESS

Naval Postgraduate School
Monterey, California 93940

12. REPORT DATE

December 1976

13. NUMBER OF PAGES

72

14. MONITORING AGENCY NAME & ADDRESS(if different from Controlling Office)

Naval Postgraduate School
Monterey, California 93940

15. SECURITY CLASS. (of this report)

Unclassified

15a. DECLASSIFICATION/DOWNGRADING SCHEDULE

16. DISTRIBUTION STATEMENT (of this Report)

Approved for public release; distribution unlimited.

17. DISTRIBUTION STATEMENT (of the abstract entered in Block 20, if different from Report)

18. SUPPLEMENTARY NOTES

19. KEY WORDS (Continue on reverse side if necessary and identify by block number)

EPSILON

$C_s^2 \cup B_T 2$

20. ABSTRACT (Continue on reverse side if necessary and identify by block number)

Shipboard measurements of temperature and velocity fluctuations were performed to determine optical propagation properties of the marine boundary layer. Empirical expressions describing the temperature structure parameter, C_T^2 in terms of the Richardson number, Ri, overland were used to evaluate data obtained for open ocean conditions. Profiles of the dissipation of turbulent kinetic energy, ϵ with respect to height, Z, and with respect to a stability parameter, Z/L, were examined for open ocean conditions.

DD FORM **1473** EDITION OF 1 NOV 68 IS OBSOLETE
1 JAN 73
(Page 1) S/N 0102-014-6601 |

251450

$C_{sub} T2$

C_T^2

In general, there was little correlation between the measured C_T^2 and the stability parameter. However, the distribution of ε with height for both the stable and unstable cases showed little deviation from that expected for near neutral conditions.

ACCESSION for

NTIS	White Section	☑
DOC	Buff Section	☐
UNANNOUNCED		☐
JUSTIFICATION		

BY
DISTRIBUTION/AVAILABILITY CODES

Dist.	AVAIL. and/or SPECIAL	
A		

DD Form 1473
1 Jan 73
S/N 0102-014-6601

2

An Examination of Turbulent Dissipation

in the Marine Boundary Layer

by

George William Karch
Lieutenant, United States Navy
B.S., United States Naval Academy, 1970

Submitted in partial fulfillment of the
requirements for the degree of

MASTER OF SCIENCE IN METEOROLOGY AND OCEANOGRAPHY

from the
NAVAL POSTGRADUATE SCHOOL
December 1976

Author _____

Approved by: _____
_____ Thesis Advisor

_____ Second Reader

_____ Chairman, Department of Meteorology

_____ Dean of Science and Engineering

ABSTRACT

Shipboard measurements of temperature and velocity fluctuations were performed to determine optical propagation properties of the marine boundary layer. Empirical expressions describing the temperature structure parameter, C_T^2, in terms of the Richardson number, Ri, overland were used to evaluate data obtained for open ocean conditions. Profiles of the dissipation of turbulent kinetic energy, ε, with respect to height, Z, and with respect to a stability parameter, Z/L, were examined for open ocean conditions.

In general, there was little correlation between the measured C_T^2 and the stability parameter. However, the distribution of ε with height for both the stable and unstable cases showed little deviation from that expected for near neutral conditions.

TABLE OF CONTENTS

LIST OF TABLES

LIST OF FIGURES

LIST OF SYMBOLS

C_n^2	Refractive index structure function parameter
C_T^2	Temperature index structure function parameter
ϵ	Rate of dissipation of turbulent kinetic energy
f	Temporal frequency
g	Acceleration due to gravity
k	Wave number
L	Monin-Obukhov stability length
L_o	Outer scale, lower limit of inertial subrange
ℓ_o	Inner scale, upper limit of inertial subrange
P	Atmospheric pressure
r	Separation distance
n	Refraction index
Ri	Richardson number
$S(i)$	Spectral density, i=f or k
T_*	Scaling temperature
U	Mean horizontal wind speed
U_*	Friction velocity
θ	Potential temperature
θ_v	Virtual potential temperature
Z	Height
Z/L	Stability parameter

9

ACKNOWLEDGEMENTS

I. INTRODUCTION

The advent of more complex and complete numerical models for analyzing and predicting large scale atmospheric motion has also led to better specifications of the boundary layer. The boundary layer is that region in the first kilometer over the sea which is defined principally by turbulent transfer of momentum and heat.

Optical propagation through the atmosphere is affected by the refractive nature of the medium. In addition to the regular variation of atmospheric refractive index with height, there exist small inhomogeneities in the refractive index associated with fluctuations in the temperature and velocity of the air. These fluctuations cause random phase and amplitude distortions in propagating wave fronts and thus degrade spatial and temporal coherence in the transmission. The magnitude of the effects places limitations on optical system performance and must be included in design and execution considerations.

Descriptions of the small scale fluctuations which affect optical propagation have not been as complete nor in the quantity for the over-water regime as for the overland regime.

Initial experimental efforts to verify turbulence theory predictions were conducted over land. Measurements of wind speed, temperature, and humidity in those investigations were made from a stable platform with auxiliary instrumentation well protected from external influences. Under these conditions relatively accurate measurements of wind speed, temperature and humidity were performed under a variety of weather conditions.

The marine environment on the other hand presents a number of problems, especially in accessibility, platform stability, and sensor protection. Overwater descriptions are necessary, even though considerable progress has been made in overland investigations. The necessity exists because of the increasing evidence of the influence on atmospheric motions by features unique to the oceanic environment.

It is the purpose of this paper to compare overland and overwater results, also, to evaluate the assumption that near neutral conditions apply for both stable and unstable conditions when evaluating the variation of turbulent kinetic energy dissipation with height.

II. <u>THEORETICAL BACKGROUND</u>

A. GENERAL

Turbulence properties of interest in optical propagation are those
which could be used to describe the intensity of fluctuations in the
refractive index and that which could be used to describe the size or
scale of the refractive index inhomogeneities. The former has been re-
lated empirically to scintillation, beam wander and beam spread, and
the latter along with the former to the image resolution which is im-
portant with respect to seeing conditions. Similarity expressions re-
lating mean conditions to properties of the turbulent regimes and hence
the temperature structure function and the dissipation rate of turbulent
kinetic energy have evolved through a series of hypotheses and asso-
ciated measurements.

An important consideration within turbulence theory is whether the
turbulence is anisotropic or isotropic. In general, anisotropy exists
within large scale eddies and isotropy exists within small scale eddies.
The universal formulae considered will be valid only for isotropic
turbulence.

Anisotropic turbulence is very empirical. Every time the boundary
changes, the turbulence changes. However at high wave numbers, which
corresponds to small scale eddies, the turbulence should be independent
of the boundaries. Kolmogorov (1941) postulated that at high wave
numbers turbulence should be isotropic even though it is generated
from and embedded in anisotropic eddies of low wave numbers. If
Reynolds numbers are high enough, turbulence will adjust through inertial

13

transfer and viscous dissipation until a statistical equilibrium, independent of initial conditions, is attained. This equilibrium consists of energy transfer into the high wave number range that is equal to energy lost through viscous dissipation.

On the basis of the isotropic nature of small scale fluctuations, only one parameter is necessary to describe the intensity of the refractive index fluctuation over many scales. It is the refractive index structure function parameter, C_n^2, defined as

$$C_n^2 = [<n(x) - n(x+r)>]^2/r^{2/3} \qquad (1)$$

where $n(x)$ and $n(x+r)$ are refractive indices at two points on a line oriented normal to the mean wind direction and separated by the distance r which is less than the outer scale, L_0, the lower end of the inertial subrange, and greater than the inner scale, ℓ_0, the smallest scale of naturally occurring turbulence.

A parallel expression, which defines the temperature structure function parameter is

$$C_T^2 = [<T'(x) - T'(x+r)>]^2/r^{2/3} \qquad (2)$$

where $T'(x)$ and $T'(x+r)$ are temperature fluctuations at two points separated by the distance r. The refractive index is determinted primarily by density fluctuations and can, therefore, be related to temperature fluctuations, neglecting himidity.

C_n^2 is related to C_T^2 by the following

$$C_n^2 = [79.\times10^{-6} \ P/T^2]^2 \ C_T^2 \qquad (3)$$

14

Fortunately, both C_n^2 and C_T^2 are readily measurable by optical and meteorological means, respectively. An alternate relationship for C_T^2, which involves measurement of the rates of dissipation of turbulent kinetic energy, ϵ, and temperature variance, $\dot{\chi}$, is

$$C_T^2 = \beta \chi \epsilon^{-1/3} \tag{4}$$

where β is an empirical constant with a value of 3.2. This last form enables indirect estimates of C_T^2 to be made from mean conditions since ϵ and χ are easily related to boundary layer fluxes and, eventually, profiles if steady horizontally homogeneous conditions exist.

Expressions which relate C_T^2 to mean properties of the boundary layer are desirable because the small scale measurements are impractical to obtain in most operational or tactical regimes and situations.

Since turbulence is nearly synonymous with temperature fluctuations, it is ultimately desirable to describe mean thermal stratification in terms of atmospheric bulk stability parameters such as the Monin-Obukhov length (L). In this regard, measurements of both atmospheric mean profiles and fluxes are required for a complete determination of atmospheric transmission behavior. Profile ($\partial\bar{\theta}_v/\partial z$ and $\partial\bar{U}/\partial z$) and boundary flux ($U_*$ and T_*) parameters appear in the following expressions for Ri and L.

$$Ri = \frac{g\partial\bar{\theta}_v/\partial z}{\theta(\partial\bar{U}/\partial z)^2} \tag{5a}$$

$$L = \bar{\theta}U_*^2/gKT_{*v} \tag{5b}$$

The following similarity predictions for the dependence of ϵ and χ on momentum and heat fluxes and height were considered by Wyngaard, et al. (1971) in deriving an empirical expression for estimating C_T^2 from mean stability parameters

$$\epsilon Z/U_*^3 = f_1(Z/L) \qquad (6a)$$

$$\chi Z/T_* U_* = f_2(Z/L) \qquad (6b)$$

The form of the empirical expression for C_T^2 is obtained by direct substitution of equations (6a and b) into equation (4) yielding

$$C_T^2 = T_*^2 Z^{-2/3} f_3(Z/L) \qquad (7)$$

Furthermore since (Z/L) and Ri can be functionally related, Businger, et al. (1971), a parallel dependence on Ri can be obtained, viz.,

$$C_T^2 = Z^{4/3}(\partial\bar{\theta}/\partial z)^2 \phi_3(Ri) \qquad (8)$$

The functions f_1, f_2, f_3, and ϕ_3 in equations (6), (7), and (8) are empirical and formulated on the basis of observations of both temperature fluctuations, momentum and heat fluxes, and mean gradients of wind speed, temperature, and humidity.

The relation expressed by equation (8) provides a desired dependence of C_T^2 on more readily measured mean stability (Z, $\partial\bar{\theta}/\partial z$, and Ri). The forms of f_3 and ϕ_3 and the data obtained from the extensive AFCRL study of turbulence structure over a flat, unobstructed

Kansas plain are presented in Wyngaard. As will be shown later, available marine data does not appear to agree for f_3 as well as expected with the overland predictions, i.e. Hughes (1976). The overland predictions for f_1 and f_2 in equation (6), were as follows

$$f_3(Z/L) = 4.9(1-7(Z/L))^{-2/3}, \quad Z/L < 0$$
$$f_3(Z/L) = 4.9(1+2.75(Z/L)) \, , \quad Z/L > 0 \qquad (9)$$

Small scale velocity fluctuation properties are of interest in optical propagation because image resolution has been empirically related to the innerscale, ℓ_0, which is defined

$$\ell_0 = (\gamma_3^1/\epsilon)^{1/4} \qquad (10)$$

where γ is the kinematic molecular viscosity and ϵ is the dissipation rate of turbulent kinetic energy similar to C_T^2. ϵ can be obtained from either one-dimensional velocity variance spectral estimates in the inertial subrange or from velocity structure function estimates.

ϵ and ℓ_0 can be functionally related to mean profile and flux estimates (U_*, T_* and Ri or Z/L) on the basis of the empirical expression presented previously (equation 6a). For the purpose of examining overwater ϵ results from different stability conditions described by Richardson numbers (Ri), equation (6a) can be expressed as follows

$$\epsilon = U_*^3/Kz \, \phi_1(Ri) \qquad (11)$$

Since Z/L and Ri are functionally related.

17

Overwater ϵ values can also be evaluated on the basis of U_* values estimated from them. Such estimates can be evaluated by comparing them with U_* estimates computed from mean wind profile measurements. Both U_* estimates utilize the following expression for the mean wind gradient

$$\partial \bar{U}/\partial z = U_*/kz \ \phi_1(Ri) \tag{12}$$

where $\phi_1(Ri)$ is defined in equation (11). $\phi_1(Ri)$ is equal to 1.0 under neutral conditions. U_* is assumed to be a constant with height in this expression so it is restricted to the constant surface layer.

Integration of equation (12) for near neutral conditions yields

$$\bar{U} = U_*/k \ \ell n \ Z/Z_0 \tag{13}$$

where U_0 is assumed equal to zero, Z_0 is the roughness parameter. The logarithmic profile suggested by equation (13) is altered by stability, shown in Figure 1. Z_0 can be eliminated from equation (13) by selecting mean winds at two appropriate levels so that

$$U_*^{'} = k(\bar{U}_2 - \bar{U}_1)/\ell n(Z_2/Z_1) \tag{14}$$

It is important to note that this expression relating U_* to mean wind values ($\bar{U}_2$ and $\bar{U}_1$) at two levels (Z_2 and Z_1) is applicable only for near neutral conditions ($Ri \cong 0$).

In near neutral conditions, turbulent kinetic energy production is assumed to be equal to the rate of molecular dissipation of turbulent
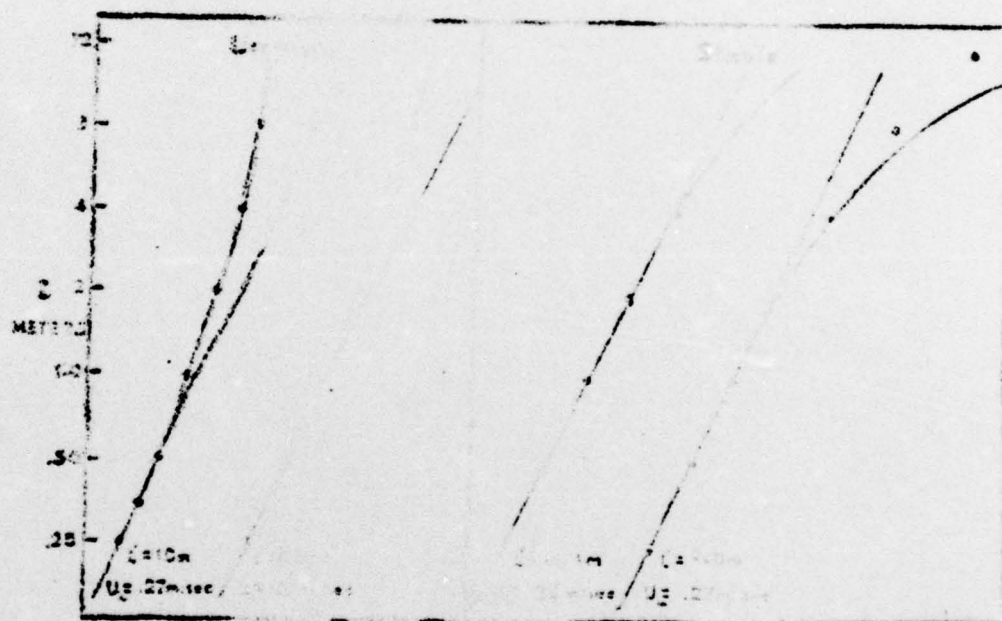
Figure 1. ...stable ...tions ...

kinetic energy and the following relation is
valid

$$\varepsilon = U_*^2 \, (\partial \bar{U}/\partial z) \tag{15}$$

combining equations (12) and (15), assuming neutral conditions $\phi_1(Ri)$ = 1.0, and solving for U_*, yields

$$U_* = (\varepsilon k Z)^{1/3} \tag{16}$$

Thus, under neutral conditions, the friction velocity (U_*) can be estimated from either mean wind profiles using equation (14) or from fluctuation data (involving turbulent energy dissipation) using equation (16).

From determined values of U_*, it is also possible to calculate a momentum drag coefficient, C_z, corresponding to a given height in the surface layer

$$C_z = U_*^2/0^2 \tag{17}$$

Numerous studies have been conducted to determine a representative value of C_z for 10 meters, Cardone (1969). Check calculations of C_{10} employing U_* determined from both mean wind profiles and dissipation rates are performed in this study.

B. STABILITY CONSIDERATIONS

Observational experiments by Businger et al. (1971) yielded a definite relationship between the Richardson number, Ri, equation (5a),

and the Monin-Obukhov length, L, equation (5b). Figure 2 from Businger, et al. (1971) lillustrates this relationship quite well. The following expressions are approximations of the relationship between Z/L and Ri, proposed by Dyer and Hicks (1970) and Webb (1970) for unstable and stable conditions, respectively,

$$Z/L = Ri \tag{18}$$

$$Z/L = Ri/1-\alpha Ri \tag{19}$$

where α is an empirically derived constant equal to 5.0.

It is important to note that Businger, et al. (1971) observed the Richardson number to approach a critical value of 0.21 as Z/L approached ∞ suggesting that as stability increases, the flow becomes essentially non-turbulent. This implies that for the surface layer the effect of mechanical turbulence becomes negligible.

The effect of hydrostatic stability on surface layer mechanical turbulence is further illustrated in Figure 3 from Businger, et al. (1971). Recalling equation (12) in light of Figure 3, it becomes apparent that the function $\phi_m(Z/L)$ vaires relatively little with respect to Z/L for unstable conditions approaching a value of 0.5. However, the rapid increase of $\phi_m(Z/L)$ as the atmosphere becomes hydrostatically stable indicates that the near neutral assumptions are invoked under only slightly stable conditions.
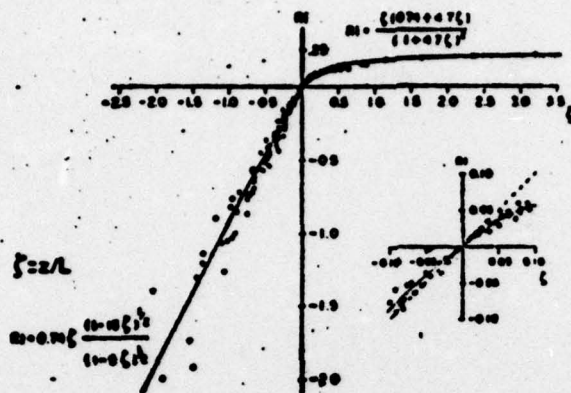
Figure 2. The dependence of Richardson number on stability.
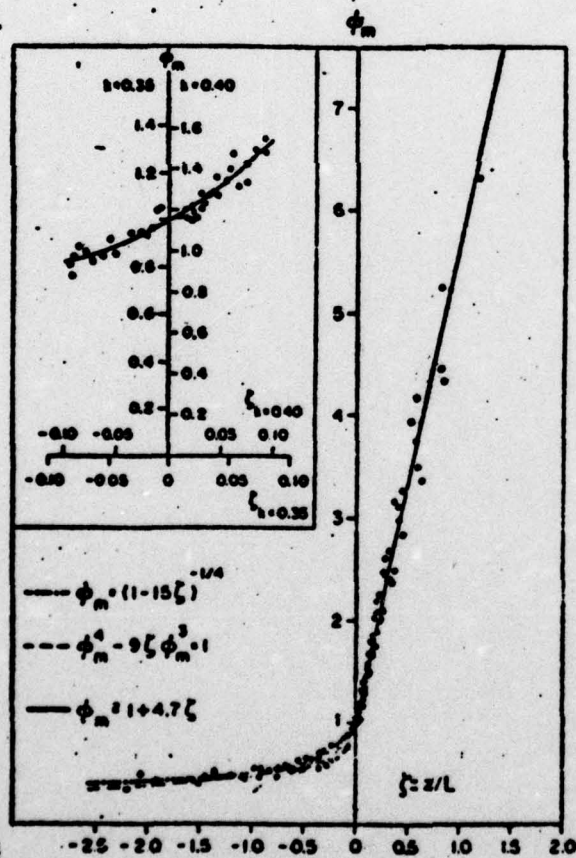
Figure 3. Comparison of dimensionless wind shear observations with interpolation formulae.

III. DATA COLLECTION

A. PLATFORM AND LOCATION

All observations were made aboard the R/V Acania while anchored in about 30 fathoms of water off Pt. Pinos in Monterey Bay. Open ocean differs from land in the effects of wave action on turbulence, in the nature of aerosols and fog, and humidity fluctuations. These conditions could best be obtained far at sea; however the cost of such activities made it desirable to work near land and the optical propagation experiments could be coincident. Pt. Pinos and other locations along the Monterey Bay shoreline provided very nearly the ideal situations for both the optical and meteorological experiments, Figure (4).

B. INSTRUMENTATION AND PROCESSING EQUIPMENT

Measurements were made at four levels. Figure 5 shows positions of the towers which support the instrumentation, length of cable runs, and position of processing and recording equipment.

The mean wind measurements were obtained with Thornwaite Associates cup anemometer wind profile register systems, model number 104. Three cups, plastic cones reinforced with aluminum frames, are mounted on stainless steel tubes attached to the main shaft at 120° intervals. When the cups rotate due to the wind a slotted shaft in the anemometer serves as a shutter between a light source and a photoelectric cell. The three cup anemometers have the characteristics of low starting speeds with a small amount of internal friction which aids in checking inertial overshoot.

23
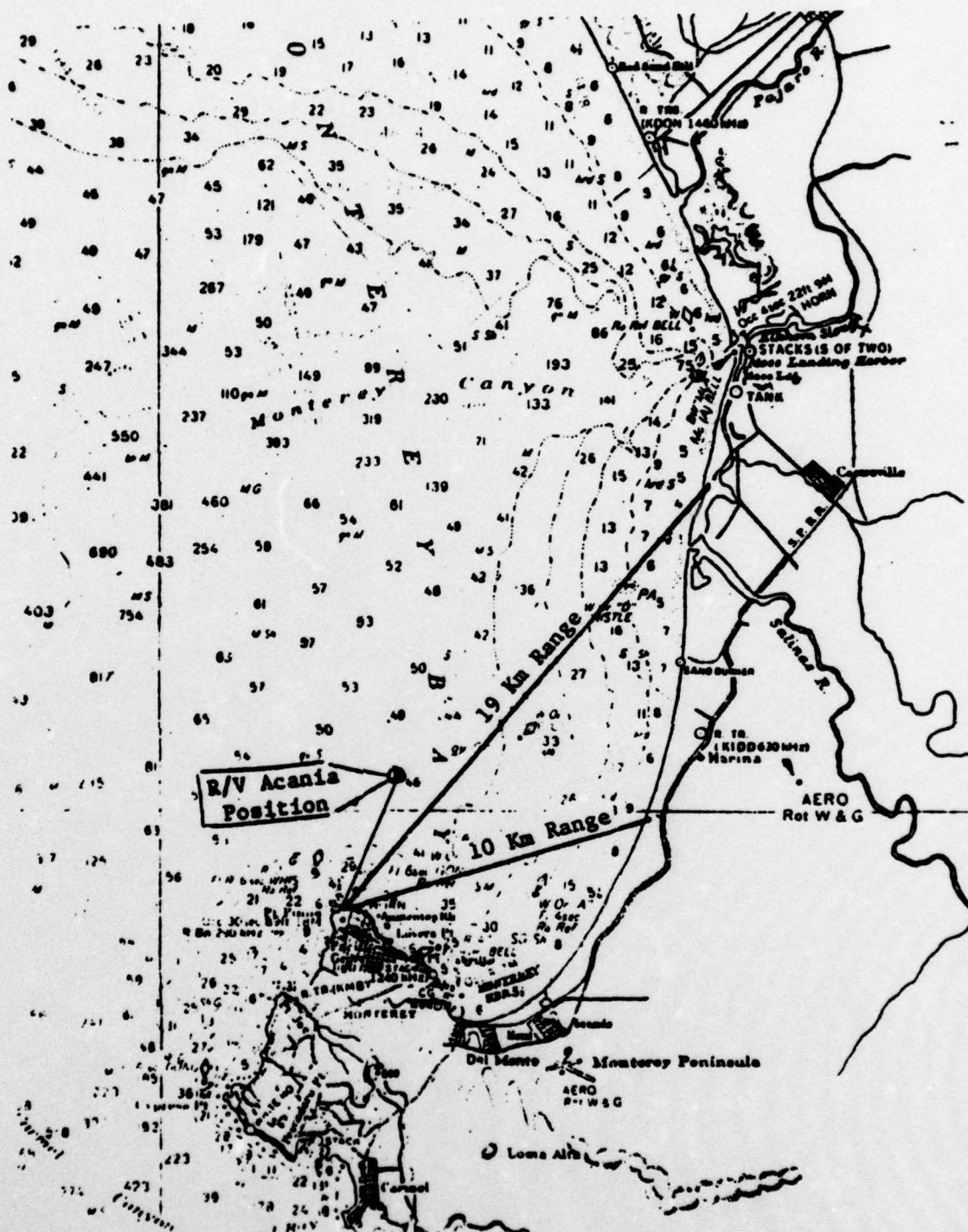
Figure 4. Optical ranges and R/V Acania position (normal) in Monterey
Bay.
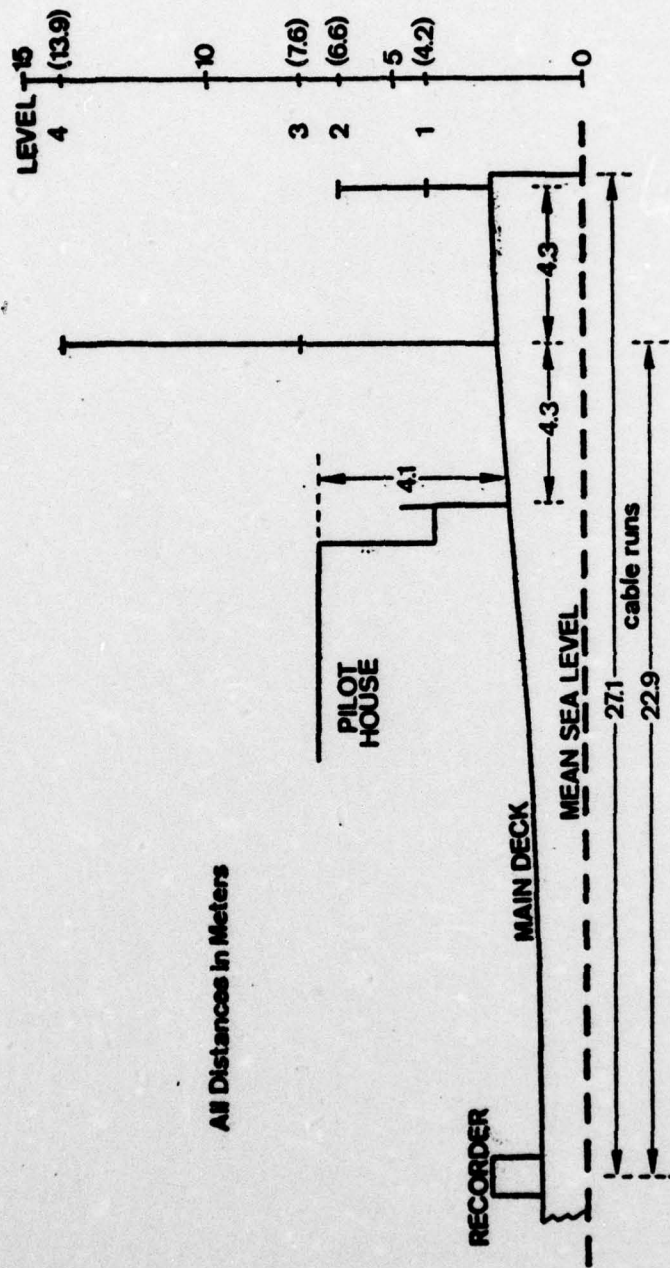
Figure 5. Sensor location on board R/V Acania.

Velocity fluctuation measurements were obtained using TSI model 1210 probes with sliding support shields and tungsten wires. The shields permitted isolation of the sensing area for the determination of the undisturbed velocity, V_o, voltage reading before and after each experiment. The platinum coated tungsten wire was small enough to resolve the viscous dissipation scale without making corrections for wire length. The wire had plated ends for isolating the sensing area and thereby minimizing flow disturbance. Figure (6)

Electronics associated with each probe were a TSI model 1054B linearized anemometer and a TSI model 1056 variable decade module. The anemometer had a linear frequency response from (dead calm) 0 KHz to 10 KHz and the variable decade module operated with a 0-60 ohm range.

Temperature fluctuations were measured using similar size sensors. A platinum wire was used in place of a tungsten wire. The temperature fluctuation system was designed for a resolution of 0.001°C at frequencies up to 1 KHz.

The temperature fluctuations were measured using a bridge developed by GTE Sylvania, the GTE Sylvania model 140. The system was slightly modified for use aboard the R/V Acania.

The baseband portion of this system is basically a balanced wheatstone bridge excited by a 3 KHz signal with a synchronous detector on the output. Segments of a very small diameter platinum wire serve as temperature sensors in opposite arms of the bridge. The resistance temperature coefficients result in an output from the bridge which is proportional to the temperature difference between the two probes. The sensor wire is 0.5 centimeters long and 2.5×10^{-4} centimeters in diameter. This extremely small mass allows a response to temperature variations

26
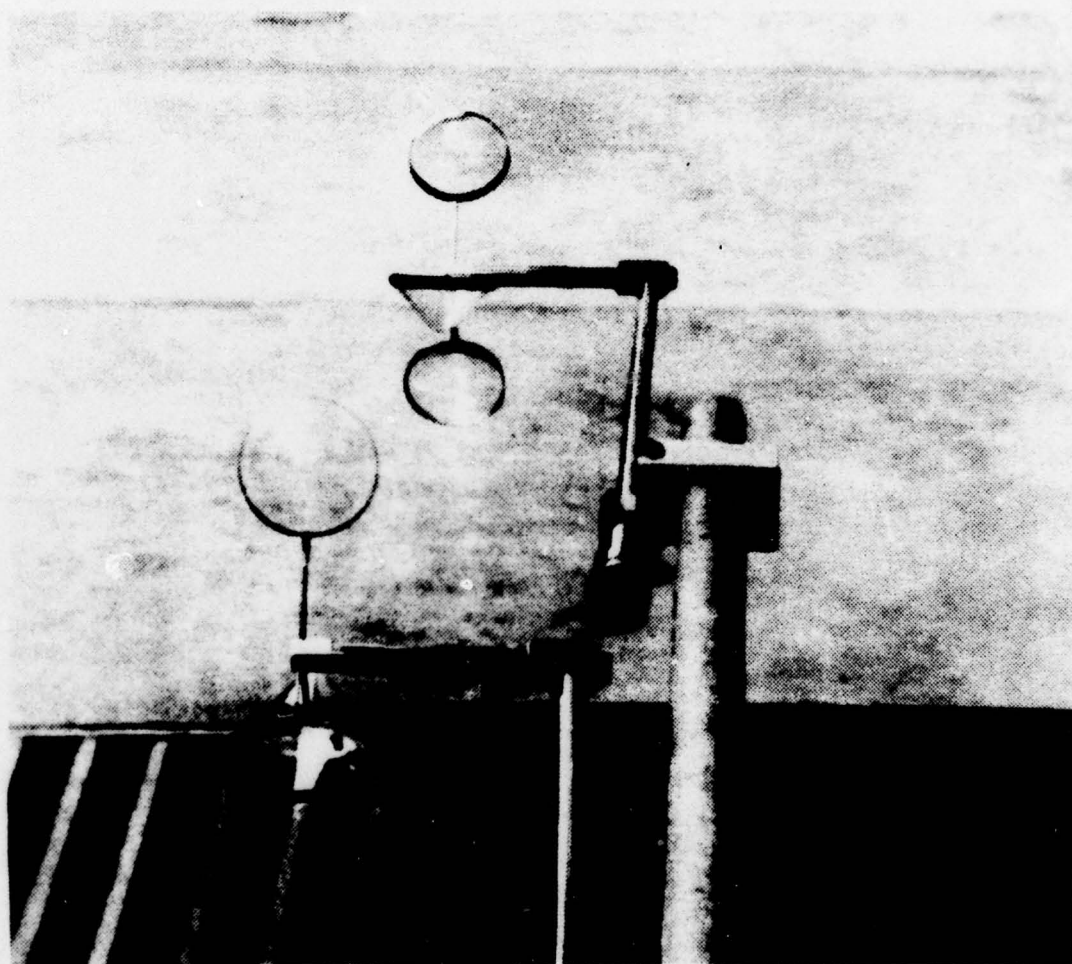
Figure 6. Thornwaite Associates cup anemometer wind profile register system.

of up to 1 KHz, while electronic amplification allows temperature differences as small as 0.004°C to be observed.

Both wind and temperature fluctuation data were recorded on a Sanborn model 3950 fourteen channel tape recorder. Real time readout on an eight channel chart recorder, brush model 240, was used to check the quality of the signals coming from the sensors. The chart data was also utilized in temperature variance analyses.

Hewlett Packard model HP-2850 temperature sensitive quartz crystal probes were used to obtain mean temperature at the sea surface and four tower levels. Figure (7) The RF signal from the probes and a reference oscillator were mixed in a Hewlett Packard HP-2801A readout unit to produce a beat frequency whose signature can be analyzed to within 0.001 °C/Hz. Each sensor received pre-experiment calibration against a platinum resistance wire thermometer in a temperature controlled circulating water bath. It was checked over the range of expected temperatures. The accuracy in achieving a 0.005°C correction factor was a constant for each probe. The tower mounted sensors were housed in aspirated shelters to eliminate radiation effects. Figure (8)

Mean relative humidity information was obtained using Dunmore type lithium chloride sensors. Figure (9) This sensor was also placed in the aspirated shelter. The basic principle of operation of this sensor is resistance change in an electrolytic solution generating a reference voltage variation proportional to relative humidity change. Automatic temperature compensation in the instruments meet the following specifications for relative humidity, $\pm$ 3% humidity below 90% and $\pm$ 4% humidity above 90%. Sensor calibration was accomplished by a comparative method using a saturated saline solution in a closed container.

28
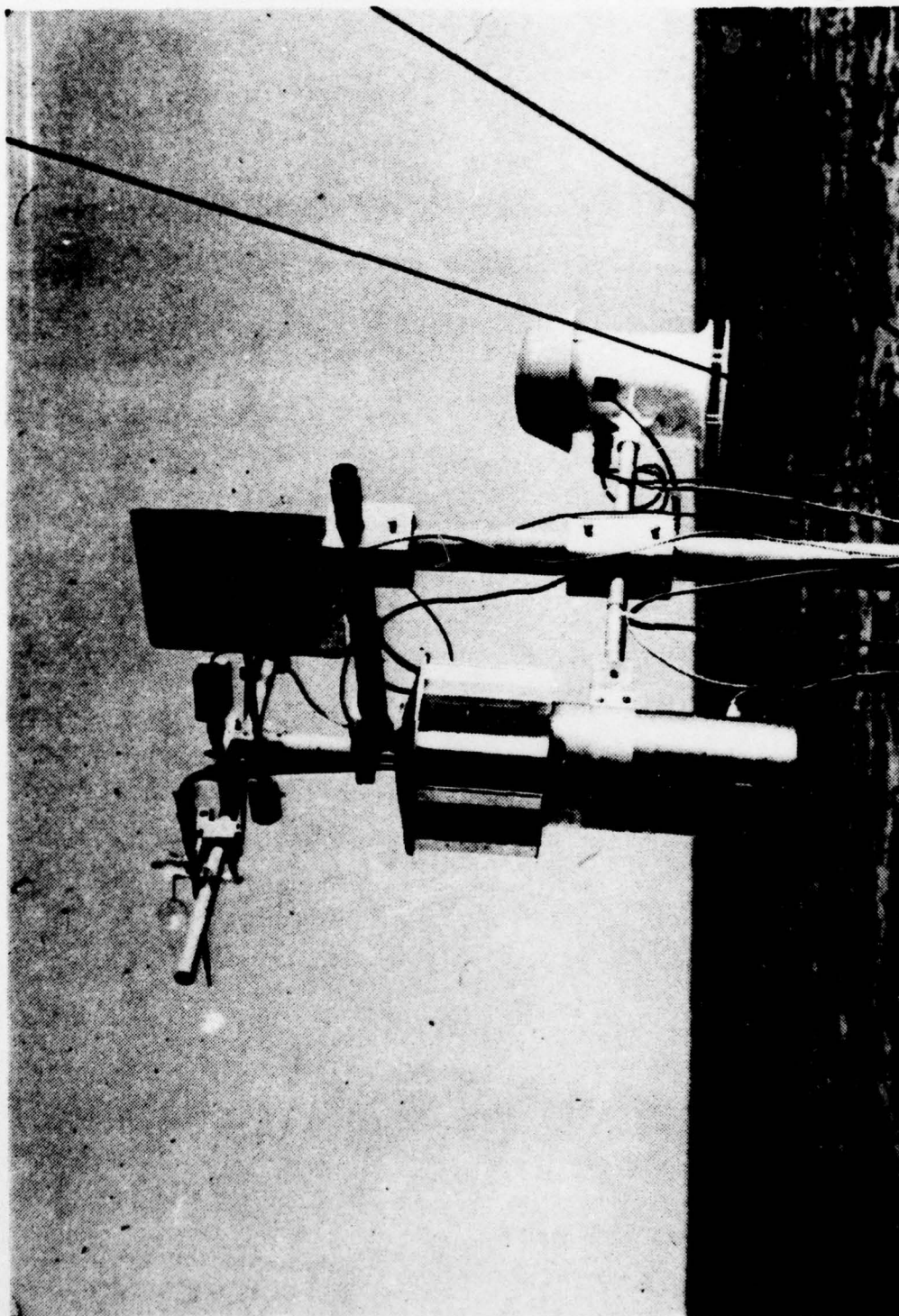
Figure 7. TSI model 1210 probes and wind vanes.
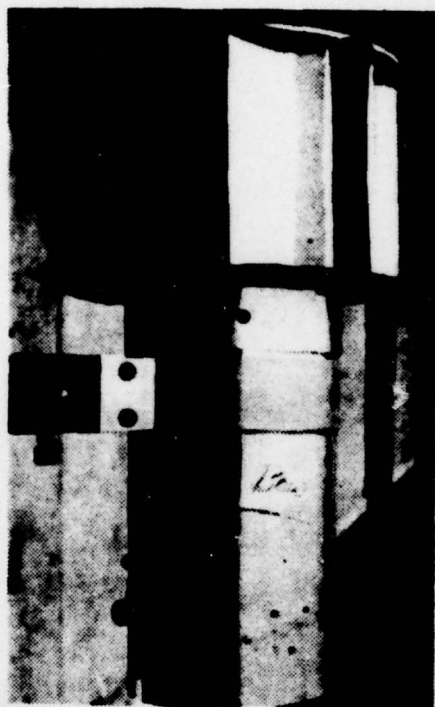
Figure 9. Aspirated shelter.
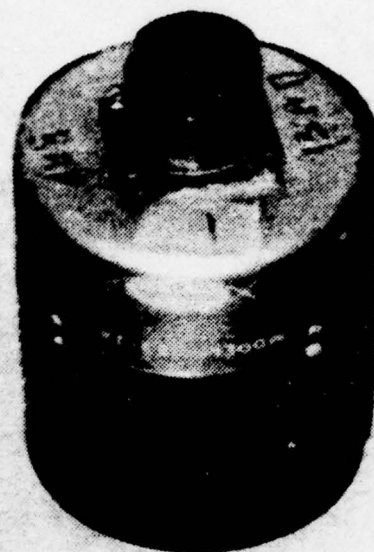
Figure 10. Dunmore type lithium chloride humidity sensor.
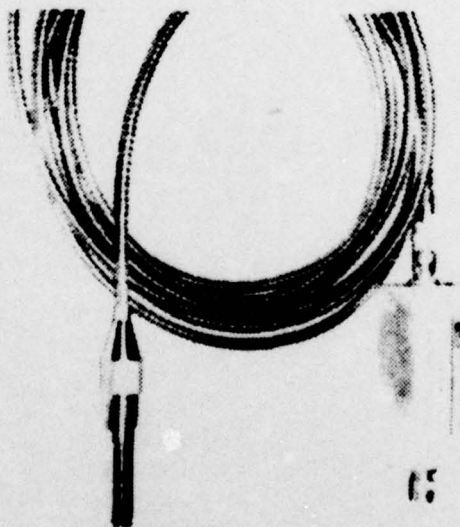
Figure 8. Hewlett Packard model HP-2850 temperature sensitive quartz crystal probes.

Sensor placement required exceptionally long cable runs. Here decrease in system frequency response due to their length had little effect in the frequency band of interest. Adjustments were made in the bridges for resistance and capacitance of the wire length.

Data logging during the experiments was accomplished using the NPS developed MIDAS (Microprogrammable Integrated Data Acquisition System). This micro-processor based data acquisition system utilizes an Intel 8008 central processor to control the sampling, averaging, and recording of mean meteorological data. All software is written in PL/M to facilitate the writing of a self-documenting program.

The operator is interfaced with the system via teletype for full duplex input/output communications and program control over the sample start time and the number of samples to be averaged before outputting. The operator may also alter the present preset sample list by adding or deleting various sensors as they come on line or become inoperable or inconsistent. Once initiated, the system is fully automated to sample the tailored list of sensors every 30 seconds and periodically print output values averaged over the selected interval of from one minute to one hour. In this study a 10 minute averaging interval was selected.

Output values were printed out on the teletype in a columnized format with the time of print as a leader. The teletype has a paper punch incorporated which may be activated by the operator to produce a data copy concurrent with the printout. This paper punch was also utilized to produce data cards for use with the IBM 360 digital computer. A magnetic cassette tape recorder has been integrated into the system

31

as a third data output device. This cassette can be interfaced to an HP 9830 portable computer so that profile and gradient flux estimates can be performed on board automatically using the basic programming capability of the HP 9830.

IV.   ANALYSES PROCEDURES

A.   ANALYSES OF MEAN DATA

Mean wind data for ten minute intervals were available from the Naval Postgraduate School developed MIDAS (Microprogrammable Integrated Data Acquisition System) output. MIDAS read values at ten second intervals and averaged them for a ten minute period. Analyses were performed on data recorded on teletype printout and also on the cassette tape.

The data was edited for gross errors or inconsistencies due to known instrumentation malfunctions. The criteria for retaining or discarding data from individual levels or for entire ten minute interval depended on performance check results obtained during measurements, obvious inconsistencies between levels and sequential times, and the availability of fluctuation data. After mean data were obtained for ten minute intervals and passed preliminary editing for obvious erroneous values, it was processed for three applications, i.e., mean wind $\bar{U}$, mean temperature $\bar{T}$, and mean humidity $\bar{q}$. These values were plotted on 2-cycle logarithmic paper. Since $\bar{U}$, $\bar{T}$, and $\bar{q}$ are expected to vary logarithmically with height, a best fit straight line should describe the distribution of data points.   Best fit lines were used to estimate gradient parameters and the Richardson number (equation 5a, Figures 10 and 12). In general, the procedures were subjective and in some instances, best fit lines with different slopes could be visualized for a given set of data points. Therefore, one criterion used was not to

33

give a single data point too much influence in determining the best fit line. Consequently, the line drawn represented a most probable position between data points without necessarily coinciding with any point (Figure 12).

B. ANALYSES OF FLUCTUATION DATA

Spectral analyses to obtain C_T^2 and ϵ values were performed on fluctuating velocity and temperature data obtained with single wires oriented in the vertical normal to the mean wind. These data represent a point measurement and yield temporal or time descriptions of the fluctuations. Twenty-one minute segments of data originally recorded on magnetic tape were recorded into the EMR-Schlumber model 1510 digital spectrum analyzer. Procedures for converting spectral values, obtained with the analog spectral analyzer, to engineering units and for obtaining turbulence parameters from the spectra are described in the following paragraphs.

A necessary procedure was to scale the spectral plots in order to relate rms input voltages to power spectral densities (PSD), variance per unit frequency. To obtain PSD levels, corresponding to rms voltage input, calibrated scales charts had to be constructed.

For purposes of the X-Y plot format of the analyzer output, the rms voltages were converted to $y = \log_{10}$ (voltage) units and a graduated scale was constructed enabling the logarithm of rms volts to be interpolated from the spectral plots. The vertical scale, Y, values from the plots were adjusted for each spectrum as a function of input and spectral gains. The values were then converted to PSD levels for use in calculating turbulence parameters. The relation used was

$$S(f) \text{ \{PSD units\}} = \frac{(\text{cal. level } V_{rms})^2}{1.5 \text{ bandwidth}} \times (10^Y)^2 \quad (20)$$

34
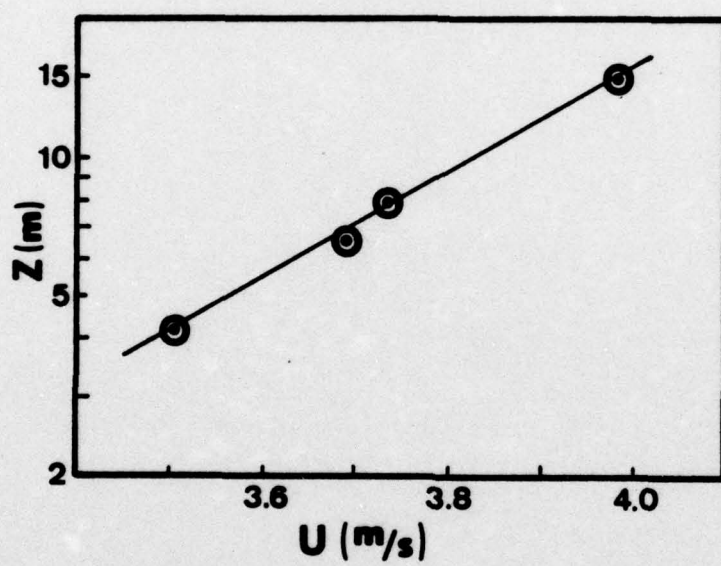
Figure 11. Mean wind profile.
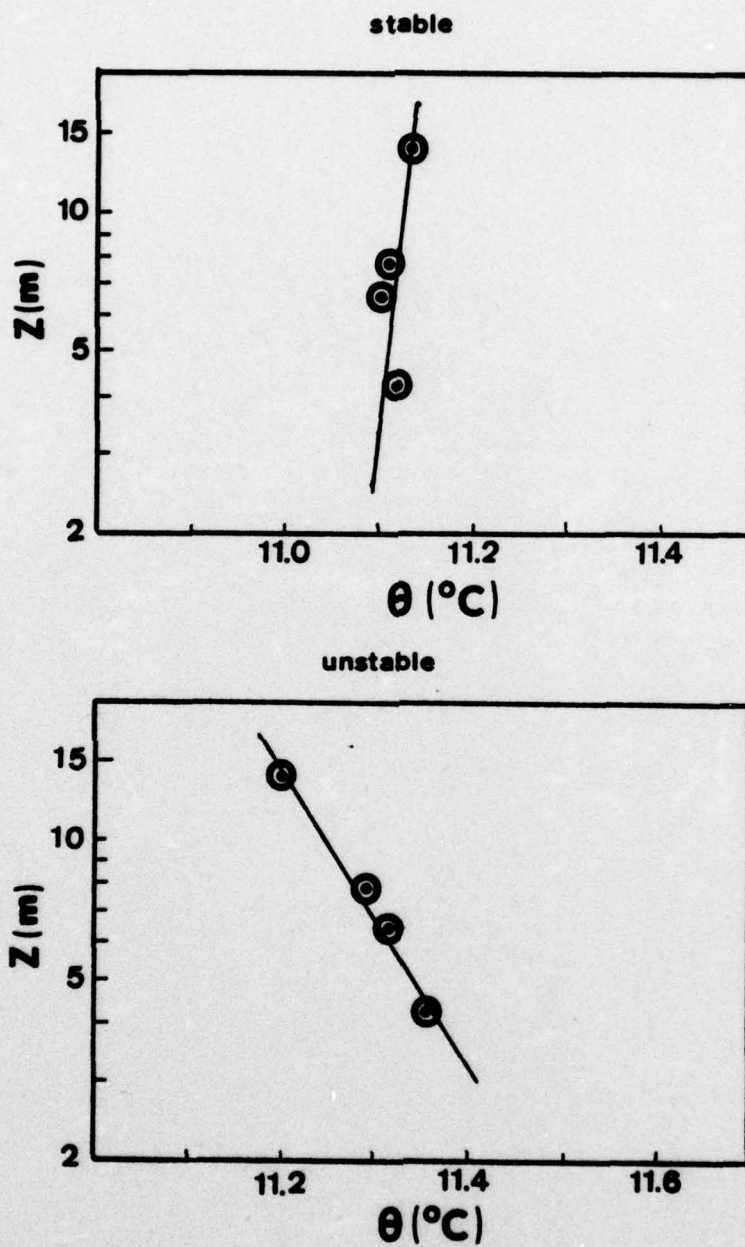
Figure 12. Potential temperature profiles.
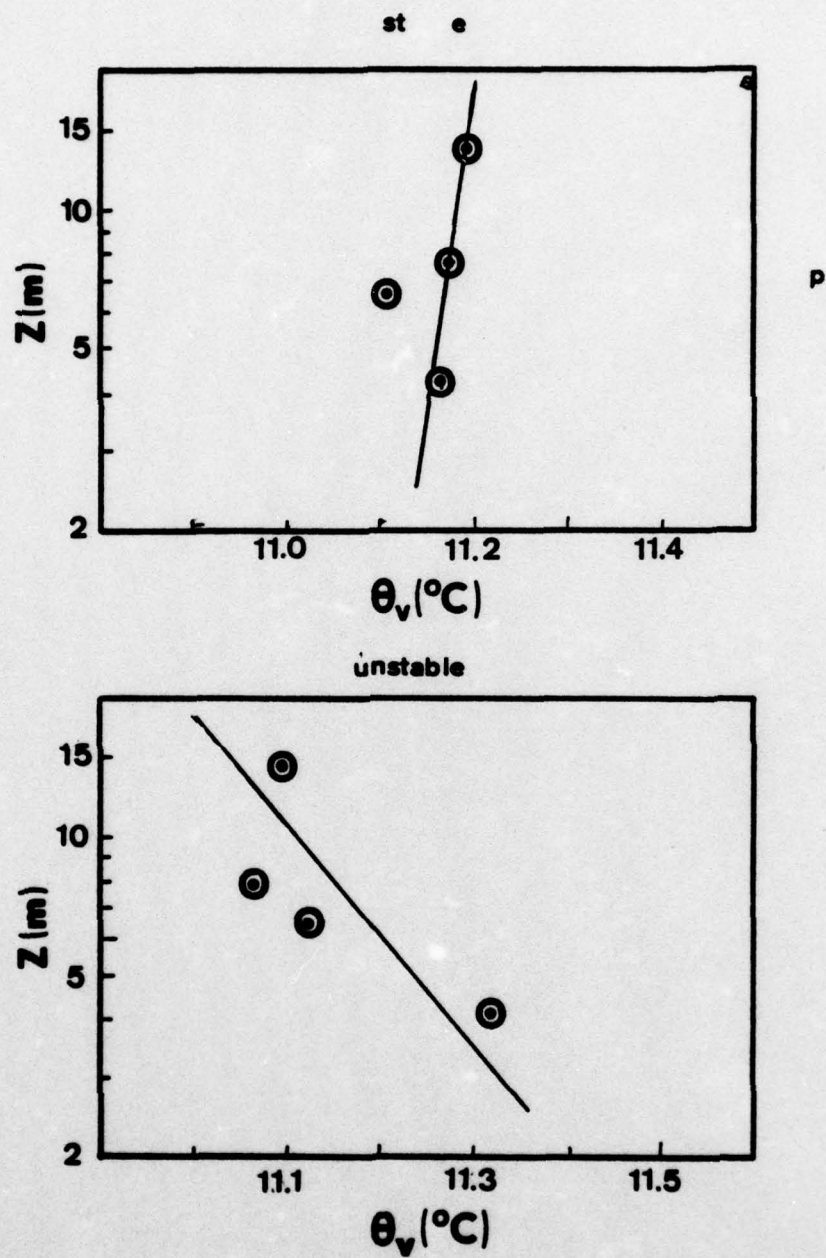
Figure 13. Virtual potential temperature profiles.

37

where bandwidth is the frequency range divided by the number of channels

$$BW = \frac{Freq\ range}{Number\ channels}$$

$$= 256\ Hz/256 = 1\ Hz$$

The calibration level volts rms equals the voltage at Y=0. (1 volt rms for a 3.16 volt input setting).

Amplitude scaling calibrations were accomplished using externally generated white noise. Signals with a 1 volt rms over a frequency range of 0.1 Hz to 1000 Hz, giving a PSD of 10^{-3} v^2/Hz. Setting a 3.16v (10 dB) input gain on the spectrum analyzer insures that 1 volt input corresponds to Y=0. An example of such a calibration plot is shown in Figure (15).

The turbulence parameters C_t^2 and ϵ were obtained from the variance spectra on the basis of the universal formulae for the inertial subrange in wave number space. These expressions predict a -5/3 slope for variance spectra of both velocity and temperature when plotted in log-log format. Figures 14 and 15 are typical spectra considered in analyses. The velocity variance spectra have consistent -5/3 slope. However, temperature spectra often exhibited slopes slightly different from the expected value of -5/3. This feature of temperature spectra has been observed by others and the existence of "cold spikes" in the temperature traces has been postulated as a probable cause, Friehe (1976).

Assuming -5/3 slopes for the variance specta, the intercept of the slope with the 1 Hz frequency line was the power spectral density value used in computing the parameter of interest, ϵ and C_t^2.

38
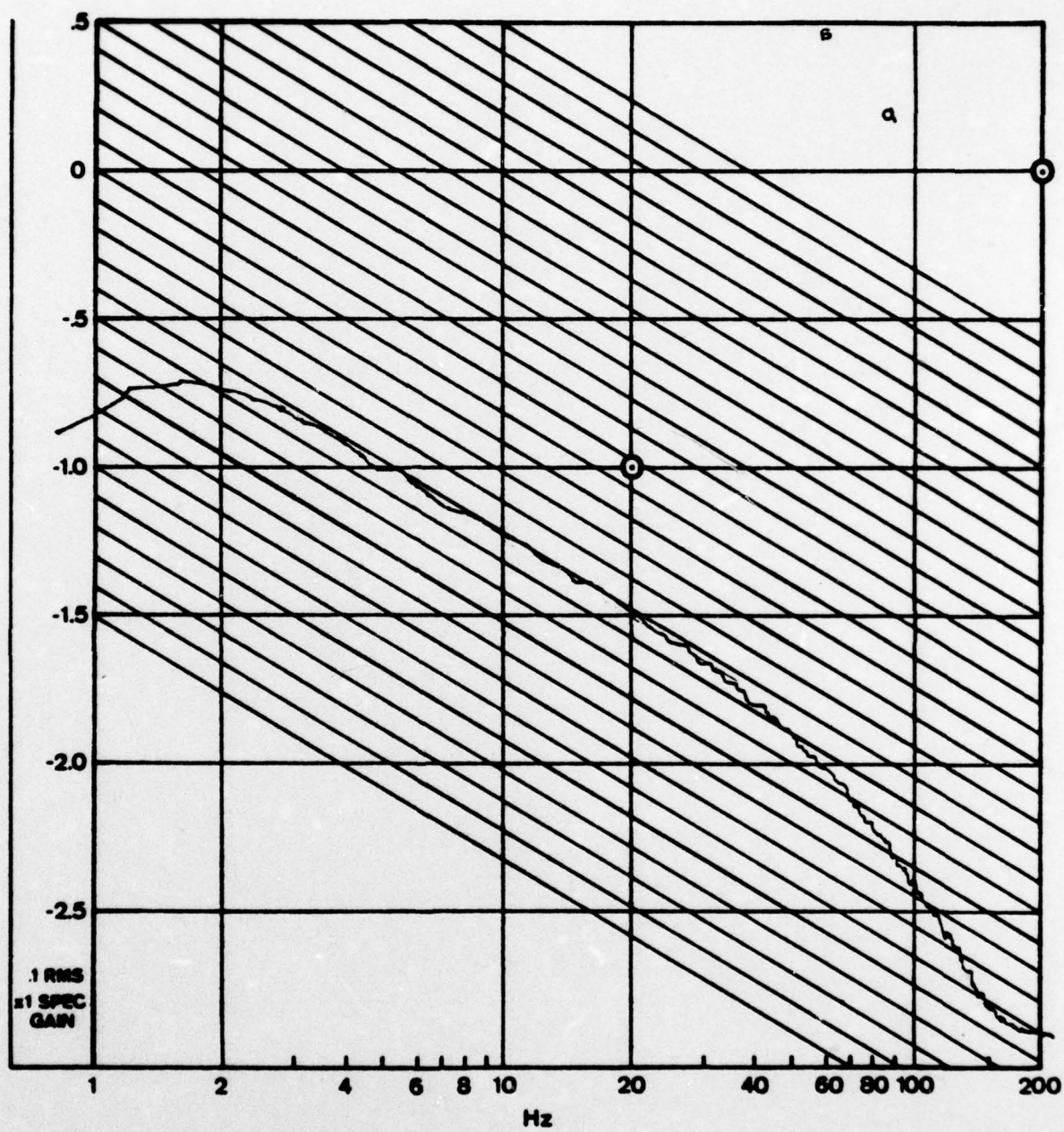
Figure 14. Velocity spectrum.
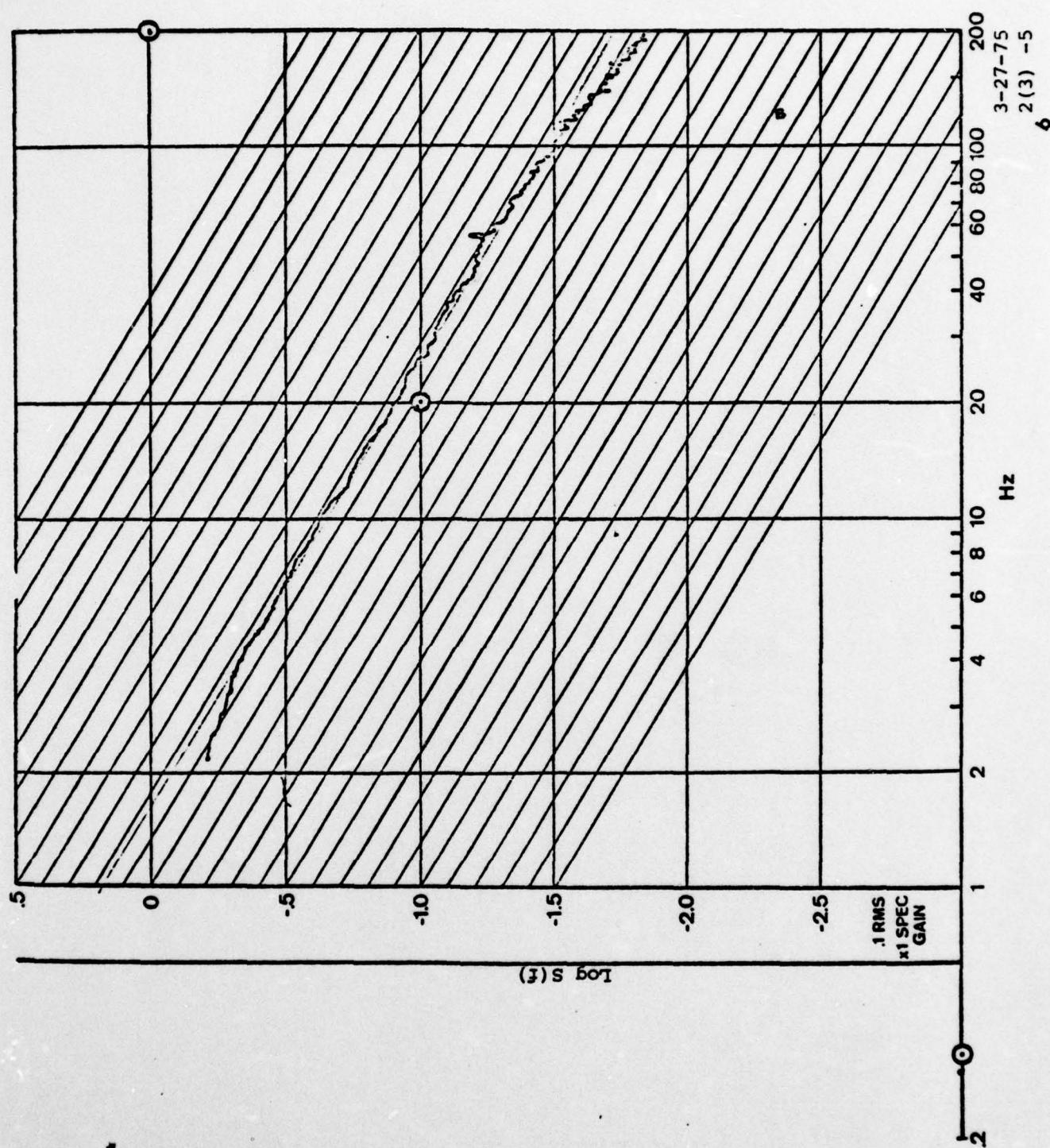
Figure 15. Temperature spectrum.

.5

0

-.5

-1.0

-1.5

-2.0

-2.5

1 RMS
x1 SPEC
GAIN

1   2   4   6 8 10   20   40   60 80 100   200

Hz
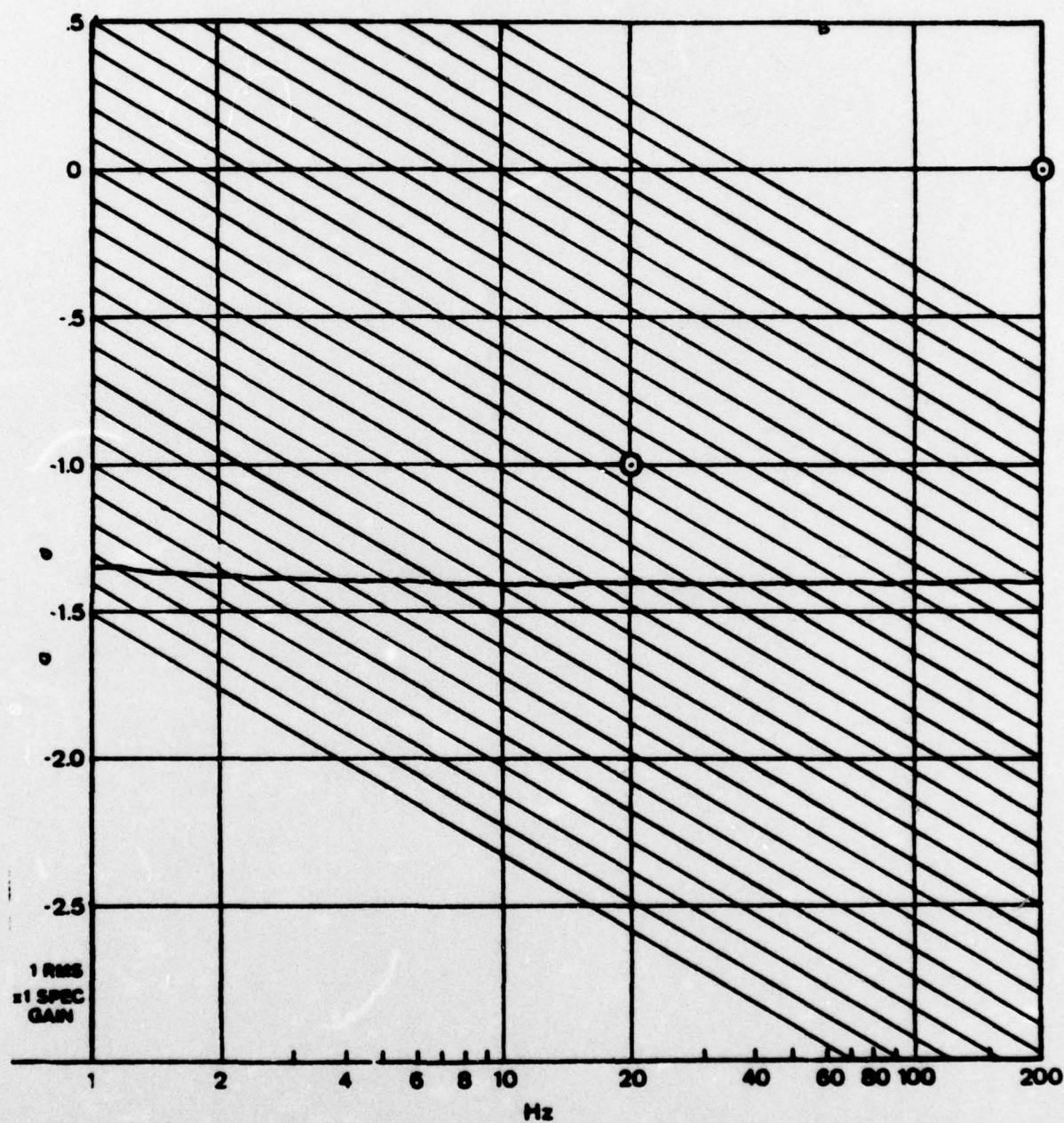
Figure 16.   Spectrum calibration plot.

41

The measured PSD value obtained from velocity spectra was converted to a spectral density in engineering units by the equation

$$S_u(f) = C_u^2 \cdot PSD$$

$$= (cm/s/volt)^2 \cdot volt^2/Hz = (cm/s)^2/Hz$$

$$(21)$$

where C is the hot-wire calibration factor. Similarly, the equation used to convert PSD values obtained from temperature spectra to dimensional values was

$$S_T(f) = C_H^2 \cdot PSD$$

$$= (°C/volt)^2 \cdot volt^2/Hz = °C^2/Hz \qquad (22)$$

where C_H is the calibration factor for the temperature system.

Since velocity and temperature fluctuations were measured at a fixed point in the flow, the resultant spectral estimates correspond to "temporal" frequencies, f, as indicated by the notation $S_u(f)$ and $S_T(f)$ in the two preceding equations. To obtain ε and C_t^2 values, temporal (f) and space (k) scales must be related in order to use equations (21) and (22). This is accomplished by Taylor's (1938) "frozen turbulence" hypothesis, that is

$$k = 2\pi f/\bar{U} \qquad (23)$$

where $\bar{U}$ is the mean wind at the measurement level. The term "frozen"

implies the turbulence pattern remains unchanged as it sweeps past the sensor probe.

The following identies are those used to relate temporal spectral estimates to spatial spectral estimates

$$f \cdot S_u(f) \equiv k \cdot S_u(k) = C_1 \, \epsilon^{2/3} \, k^{-2/3} \qquad (24)$$

$$f \cdot S_T(f) \equiv k \cdot S_T(k) = C_2 \, C_T^2 \, k^{-2/3} \qquad (25)$$

where $S_u(f)$ and $S_T(f)$ are spectral density values with units of $(m/s)^2/Hz$ and $°C^2/Hz$ respectively. The above equations are rewritten in the following forms to obtain ϵ and C_T^2 from values of f, $\bar{U}$, $S_u(f)$, and $S_T(f)$

$$\epsilon = \{ \frac{k^{2/3}}{C_1} \cdot f \cdot S_u(f) \}^{3/2} \qquad (26)$$

$$C_T^2 = \{ \frac{k^{2/3}}{C_2} \cdot f \cdot S_T(f) \}^{3/2} \qquad (27)$$

where $k = 2\pi f / \bar{U}$ and $C_1 = .5$ and $C_2 = .25$, empirically.

C. ANALYSES OF PAIRED TEMPERATURE SENSOR

C_T^2 values were also estimated by using paired sensors for variance analyses. This analysis was based on the expression for the temperature structure function, equation (2).

The analysis is one in which temperature differences between paired resistance wires separated by a distance r is subjected to variance analyses as indicated by the term $[T'(x)-T'(x+r)]^2$ on equation (2).

43

Voltages corresponding to the temperature differences, ΔT, as measured by the paired sensors were recorded on analog magnetic tape. During experimental periods, calibration voltages were also recorded on the data tape for reconstruction of the signal. This calibration signal was played back at the time of data analysis to provide a reliable check of the recording system performance in both record and playback modes.

The variance or mean square of the temperature differences required to compute C_T^2 was obtained by analyzing the analog voltages with a mean square voltmeter (Thermo Systems Incorporated, model 1060) using a 30 second time constant for the averaging. The output of the mean square voltmeter as well as a record of the original signal were recorded on standard strip charts. A strip chart section appears in Figure 17. The record of the original instantaneous signal provides an important means of spotting extraneous noises. The rms voltmeter-strip chart recorder system was also calibrated using known input voltages. At least one input calibration voltage was larger than the largest expected signal on the data record and likewise one input calibration voltage was lower than the smallest expected signal. This procedure minimized any non-linearities in either the rms voltmeter of the strip chart recorder.

Five minute averaged values of the rms voltages were abstracted from the strip chart and these values are utilized in a program for the IBM 360 computer. This program converts the mean square voltages values to temperature difference variances values, from which C_T^2 was computed. A final check on the validity of the measured data was made by performing spectral analyses on representative data samples from each experimental run. The spectrum analyzer, described in section B, was used to
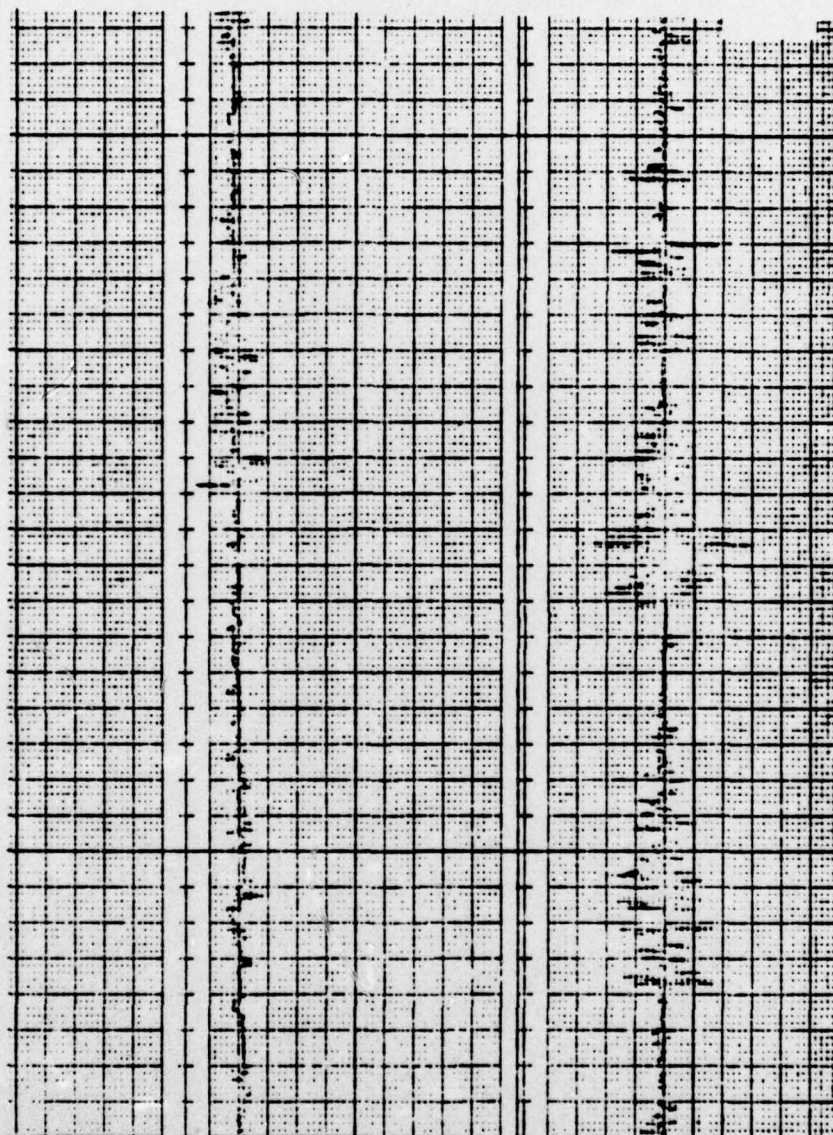
Figure 17. Sample strip chart section.

obtain the spectra which were subsequently plotted and kept as a permanent record. Any harmonic noise appeared as a spike in an otherwise reasonably smooth curve. It should be emphasized that continuous calibration and data checking procedure were essential steps throughout the analyses.

D. HOT WIRE CALIBRATION

In-situ calibrations of the velocity sensors were accomplished every 10 minutes during the experiment. In this procedure recordings were made of both the cup anemometer wind speed and the corresponding hot wire voltage output. The sensor wind speed is given by

$$V^2 = a \, \overline{U}^{1/2} + b \tag{28}$$

where V is the hot-wire voltage output and $\overline{U}$ is the mean wind speed for any given level. The constants, a and b, are the calibration curve slope and intercept respectively. The constants, a and b, are derived from the in-situ calibration curve.

To convert the voltage PSD levels to velocity units requires a calibration factor given by

$$\dot{U}' = Cv' \tag{29}$$

where C is the calibration factor in m/s /volt, v' is the voltage fluctuation, and U' the velocity fluctuation. Differentiating equation (28) yields

$$\dot{U}' = (4v\overline{U}^{1/2}/a) \, v' \tag{30}$$

which when substituted into equation (29) yields

$$C = 4v\overline{U}^{1/2}/a \qquad\qquad (31)$$

An example in-situ calibration curve is shown in Figure 18. The slope of the curve yields the value for a in equation (31).
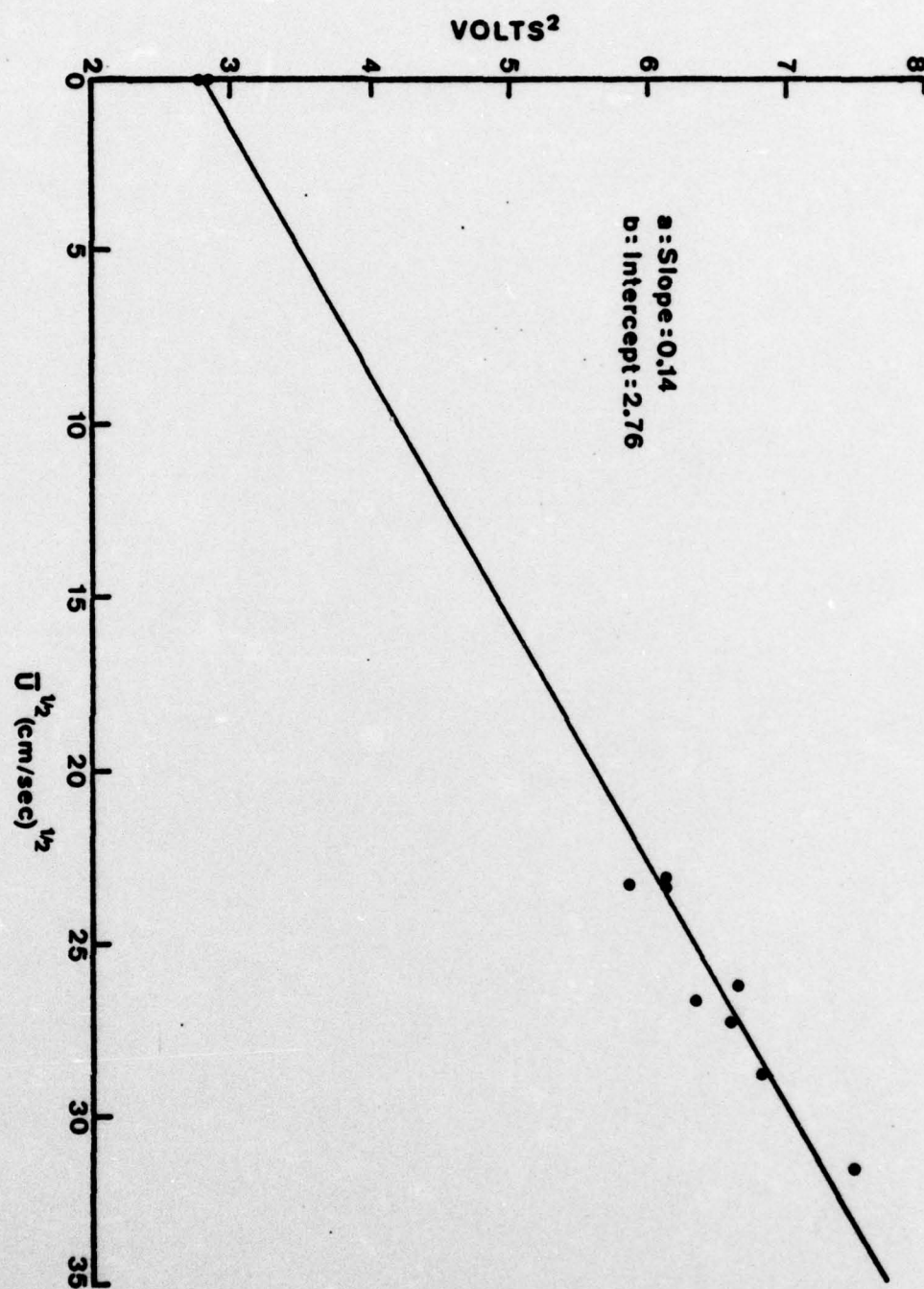
Figure 18. In-situ calibration plot.

V. RESULTS

A comparison of the observed overwater results and those obtained
by Wyngaard, et al. (1971) appear in Figures 19, 20, respectively.
In each case dots represent an individual data point. For the overwater
results mean values over Ri intervals of 0.25 were determined, plotted
in the center of the interval, and appear as small dots within circles.
Error bars delineate one standard deviation from the mean within each
interval. The number at the top of each error bar is the number of
data points used in defining the mean in the interval.

For the stable and unstable regime with $0.5 > Ri > -0.5$ there is
some correlation with the results of Wyngaard, et al. However, for
$Ri < -0.5$ there is little agreement with the difference in results on
the order of one order of magnitude. There is some agreement with the
trend in the sense that it does not change significantly with
instability.

Many of the Richardson numbers were not within acceptable ranges,
for positive, and negative Ri values. Results are not included for
positive Ri values above 1.0 and negative values lower than -3.0. A
predicted critical positive Ri value can be derived from equation (19),
which gives a value of 0.21.

Scatter in the observed results could be attributed to the scatter
in both the measured C_T^2 and $\partial\theta/\partial z$ values. Deviation of tempera-
ture spectra from the -5/3 slope caused uncertainty in the C_T^2 esti-
mates. The $\partial\theta/\partial z$ values are dependent on profile estimates whose de-
termination was at times subjective as discussed in conjunction with
Figure 21.
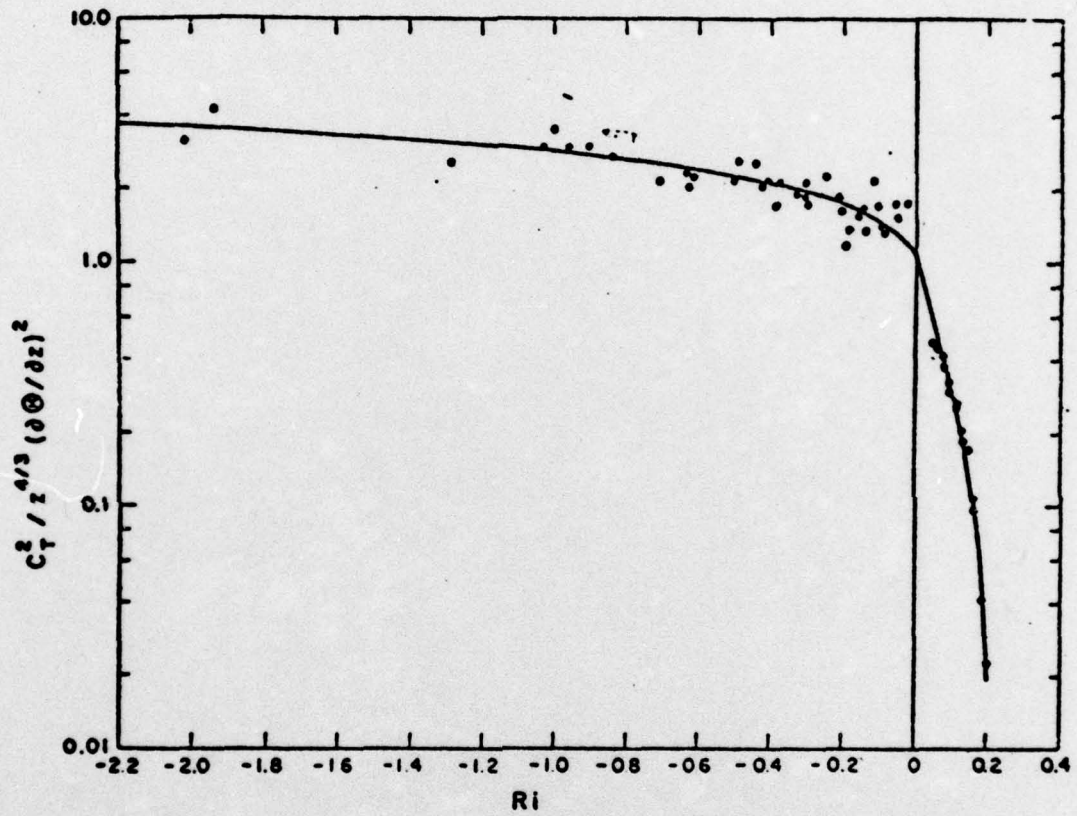
Figure 19. Wyngaard, et al. (1971) prediction curve.
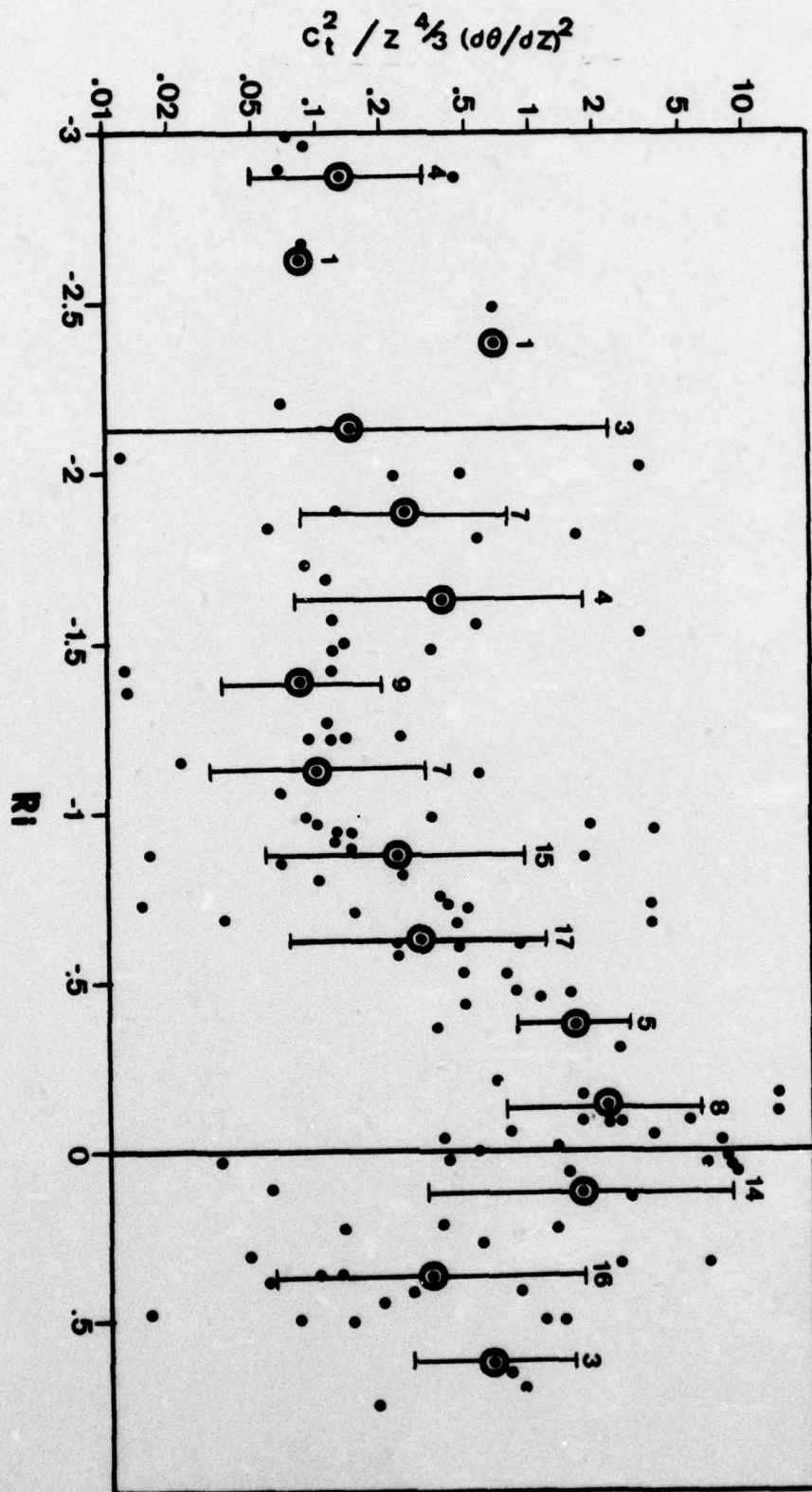
Figure 20. Observed prediction curve.

Friction velocity values, U_*, were calculated in two ways. In the first method (Method A) profiles of log (z) versus mean wind, $\bar{U}$, were plotted to obtain gradient estimate. An example profile is shown in Figure 10. After the profiles were drawn, 5 and 10 meter level wind speeds were estimated from the profiles for each 10 minute period and these values were used to solve equation (14) for U_*. These values appear in column A of Table I.

Friction velocity values were also calculated from fluctuation data (Method B). First, equation (24) was solved to obtain a value for the turbulent kinetic energy dissipation rate, ε, at each level. Then the neutral prediction, equation (16), was used to obtain a U_* at each level. Ideally U_* at all levels would be equal for any given period since U_* is assumed to be constant in the surface layer. The values, with about 10% exceptions, were within acceptable limits of each other. They were then averaged to obtain representative values for U_*. Results from these computations appear in Table I column B.

U_* values were also calculated using wind speed dependent C_{10} values suggested by Cardone (1969) and a value of U taken from profiles, at a height of 10 meters, using

$$U_* = U_{10}\sqrt{C_{10}} \tag{32}$$

Cardone's C_{10} representation was for the marine boundary layer. These values are shown in Table I column C.

The results are similar to those reached by Atkinson (1976), i.e., showing some disagreement between U_* values obtained by the two methods, with the fluctuation data method more closely agreeing with Cardone's results.

52

TABLE I

Comparison of U_* values.

U_*
(m/s)

A	B	C
.29	.20	.18
.29	.19	.18
.27	.19	.17
.21	.21	.15
.30	.21	.14
.26	'.21	.14
.25	.22	.14
.21	.26	.17
.19	.24	.15
.19	.24	.15
.08	18	.15
.15	.16	.15
.26	.20	.15
.18	.17	.12

METHOD:

$$A - \quad k(U_2 - U_1) / \ln(Z_2/Z_1)$$

$$B - \quad (\epsilon kz)^{1/3}$$

$$C - \quad U_{10}(C_{10})^{1/2}$$

53

The normalized dissipation rate $K \epsilon Z U_*^{-3}$ in relation to Z/L was tested in the same manner as Garratt (1972). The results of Garratt (1972) and those obtained in this study are shown in Figures 22 and 23, respectively. The curve represents the function $\phi_m(Z/L) - Z/L$. Similar scatter was also observed in an investigation by Busch and Panofsky (1968).

An examination was also made of the variation of the observed dissipation rate of turbulent kinetic energy, ϵ, with height for the different stability conditions. Results of this appear in Figures 24 and 25 for stable and unstable conditions, respectively. The results from both stability regimes are compared to the -1 properties for neutral stability. The results show that for all stability conditions a slope corresponding to near neutral conditions was observed.

30 APRIL 1976
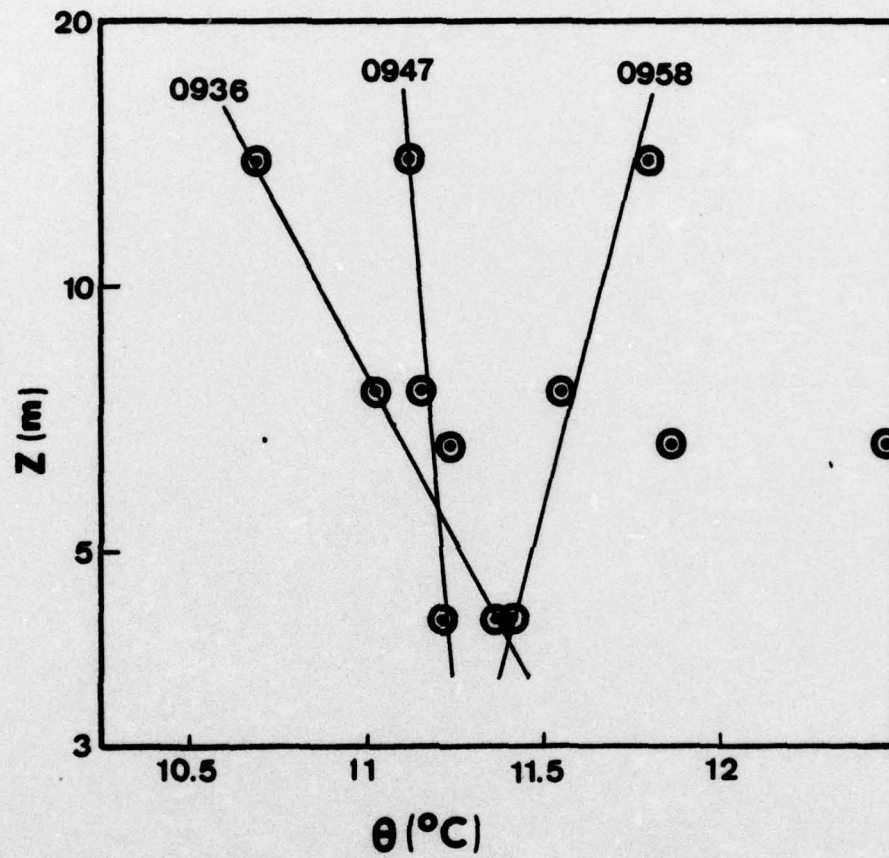
Figure 21. Erroneous profile.

From Garrett (1972)
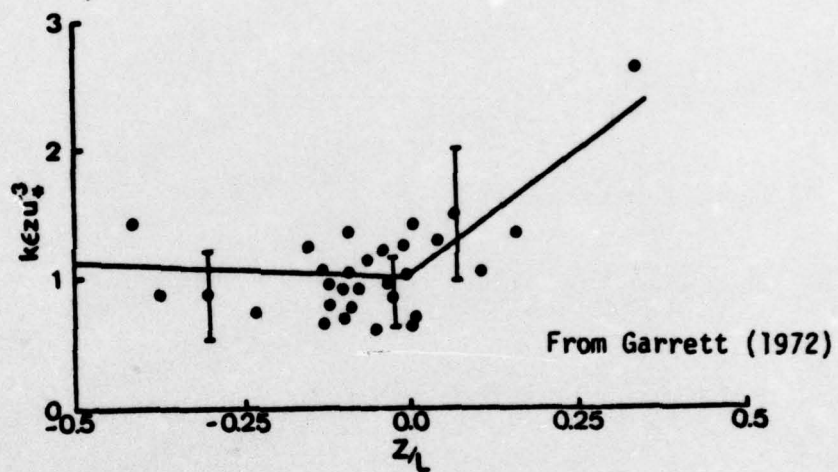
Figure 22. Garratt's results.
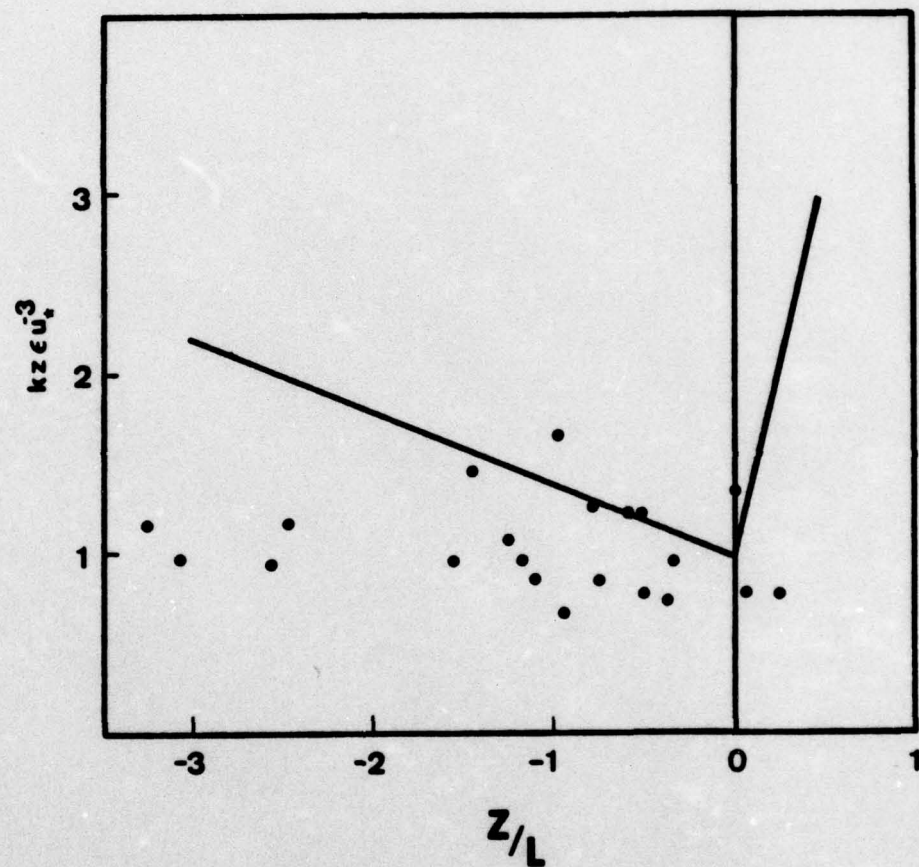
Figure 23. Observed results.

stable

Figure 24. ε versus log Z.

unstable

Figure 25. ε versus log Z.

58
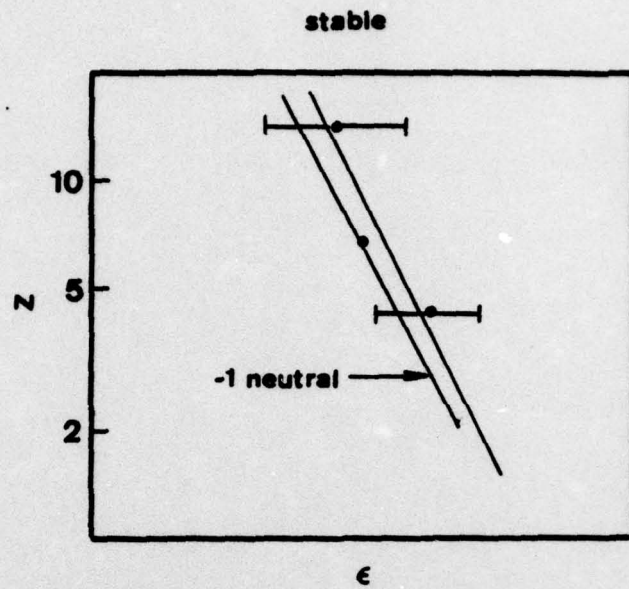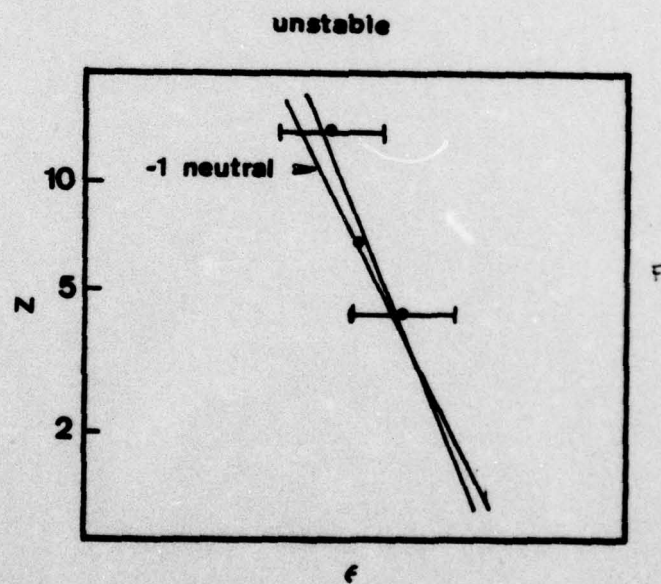
VI. CONCLUSIONS

Correlation of spectrally derived C_T^2 results with the stability parameter, Ri, was poor for the data obtained in this study of the marine environment. Verification evaluations for friction velocity results from mean (profile) and turbulent (dissipation) data were satisfactory. Correlation of normalized ε with the stability parameter (Z/L) showed the same scatter as results of others. The variation of ε with height exhibited results which support the near neutral predictions for most cases.

It is concluded that the turbulent field in the marine boundary layer is subjected to several anomalous effects which can cause the disruption of the inertial subrange. Thus, empirically, expressions for describing overland transmission characteristics will undoubtedly have to be altered to provide operational determinations for utilization in the marine environment.

$$\text{TABLE II. } C_T^2 \text{ and Ri Results.}$$

	Period	Level (M)	$d\bar{\theta}/dz$ °C/cm	C_T^2 x 10^{-3}	Ri
1974	3-27-1841	4.19	0.049	1.59	0.362
		6.60	0.031	0.94	0.500
		7.64	0.027	1.57	0.500
		13.89	0.015	-	1.000
	3-27-1902	4.19	0.047	1.97	0.249
		6.60	0.030	0.61	0.392
		7.64	0.026	2.02	0.454
		13.89	0.014	-	0.750
	3-27-1928	4.19	0.047	5.40	0.230
		6.60	0.030	1.37	0.362
		7.64	0.026	2.89	0.419
		13.89	0.014	1.20	0.750
	3-27-2117	4.19	0.019	3.45	0.073
		6.60	0.012	6.89	0.115
		7.64	0.012	-	0.113
		13.89	0.006	1.42	0.242
	3-28-1902	4.19	0.046	16.56	1.000
		6.60	0.029	-	1.500
		7.64	0.025	12.07	1.500
		13.89	0.014	1.46	1.500
	3-28-2059	4.19	0.054	56.73	0.388
		6.60	0.034	-	0.500
		7.64	0.030	14.21	0.500
		13.89	0.016	19.25	1.000
	8-13-1700	4.19	-0.036	4.33	-0.538
		6.60	-0.023	0.42	-0.847
		7.64	-0.020	0.53	-0.981
		13.89	-0.011	0.23	-1.783
	8-13-1721	4.19	-0.036	3.76	-0.665
		6.60	-0.023	0.42	-1.047
		7.64	-0.020	0.67	-1.213
		13.89	-0.011	0.27	-2.204

	Period	Level (M)	$d\bar{\theta}/dz$ °C/cm	$C_T^2 \times 10^{-3}$	Ri
1974	8-13-1742	4.19	-0.025	4.25	-0.451
		6.60	-0.016	0.45	-0.711
		7.64	-0.013	0.63	-0.823
		13.89	-0.007	0.21	-1.496
	9-18-1643	4.19	0.031	0.29	0.308
		6.60	0.020	0.08	0.486
		7.64	0.017	-	0.500
		13.89	0.009	0.11	1.000
	9-19-1735	4.19	-0.005	0.47	-0.082
		6.60	-0.003	1.18	-0.128
		7.64	-0.003	-	-0.149
		13.89	-0.001	0.56	-0.270
	9-19-1846	4.19	-0.005	5.07	-0.100
		6.60	-0.003	10.27	-0.157
		7.64	-0.003	-	-0.181
		13.89	-0.001	1.10	-0.330
	9-19-1900	4.19	-0.010	0.59	-0.607
		6.60	-0.006	0.87	-0.957
		7.64	-0.005	-	-1.107
		13.89	-0.003	0.91	-2.013
	9-19-1929	4.19	-0.005	0.73	-0.099
		6.60	-0.003	1.17	-0.156
		7.64	-0.003	-	-0.180
		13.89	-0.001	1.14	-0.328
	9-19-2011	4.19	-0.010	0.50	0.051
		6.60	-0.006	0.81	0.080
		7.64	-0.005	-	0.093
		13.89	-0.003	0.55	0.169
	9-19-2115	4.19	-0.172	0.35	-3.000
		6.60	-0.109	0.69	-3.000
		7.64	-0.094	-	-3.000
		13.89	-0.052	0.77	-3.000

	Period	Level (M)	$d\bar{\theta}/dz$ °C/cm	C_T^2 x10^{-3}	Ri
1974	9-19-2158	4.19	-0.010	0.46	-0.202
		6.60	-0.006	1.12	-0.319
		7.64	-0.005	-	-0.369
		13.89	-0.003	1.10	-0.671
	9-19-2243	4.19	-0.178	0.32	-3.000
		6.60	-0.113	0.78	-3.000
		7.64	-0.098	-	-3.000
		13.89	-0.054	1.08	-3.000
	9-20-0014	4.19	-0.011	0.66	-0.461
		6.60	-0.007	2.12	-0.727
		7.64	-0.006	-	-0.841
		13.89	-0.003	1.0	-1.530
	9-20-0056	4.19	-0.013	0.56	-0.408
		6.60	-0.008	-	-0.643
		7.64	-0.007	-	-0.744
		13.89	-0.004	1.88	-1.353
	9-20-0140	4.19	-0.013	0.77	-0.546
		6.60	-0.008	1.43	-0.860
		7.64	-0.007	-	-0.995
		13.89	-0.004	0.89	-1.809
	9-20-0530	4.19	-0.003	0.76	-0.085
		6.60	-0.002	1.77	-0.134
		7.64	-0.002	-	-0.155
		13.89	-0.001	1.68	-0.282
	9-20-0552	4.19	-0.006	0.91	-0.952
		6.60	-0.004	-	-1.500
		7.64	-0.004	-	-1.736
		13.89	-0.002	0.99	-3.000
	11-21-1800	4.19	-1.626	3.74	-3.000
		6.60	-1.032	8.85	-3.000
		7.64	-0.892	2.02	-3.000
		13.89	-0.490	5.93	-3.000

	Period	Level (M)	$d\bar{\theta}/dz$ °C/cm	C_T^2 x 10^{-3}	Ri
1974	11-21-1821	4.19	0.008	3.39	0.027
		6.60	0.005	1.97	0.043
		7.64	0.004	1.97	0.050
		13.89	0.002	2.24	0.091
	11-21-1842	4.19	0.006	3.49	0.033
		6.60	0.004	2.17	0.051
		7.64	0.004	2.11	0.060
		13.89	0.002	9.17	0.108
	11-21-1903	4.19	0.003	5.65	0.009
		6.60	0.002	3.26	0.014
		7.64	0.002	3.00	0.017
		13.89	0.001	1.24	0.030
	11-21-2027	4.19	0.002	7.75	-0.001
		6.60	0.001	1.42	-0.001
		7.64	0.001	3.61	-0.001
		13.89	0.000	0.89	-0.002
	11-21-2048	4.19	0.002	8.39	0.006
		6.60	0.001	9.75	0.010
		7.64	0.001	3.55	0.012
		13.89	0.000	1.36	0.021
	11-21-2109	4.19	-0.000	9.71	-0.025
		6.60	-0.000	7.22	-0.039
		7.64	-0.000	4.11	-0.046
		13.89	-0.000	1.19	-0.083
	11-21-2130	4.19	0.0	11.04	-0.037
		6.60	0.0	7.97	-0.059
		7.64	0.0	5.90	-0.068
		13.89	0.0	1.72	-0.123
1975	3-27-1503	4.19	0.006	10.57	0.004
		6.60	0.004	6.14	0.007
		7.64	0.004	3.43	0.008
		13.89	0.002	-	0.015

	Period	Level (M)	$d\bar{\theta}/dz$ °C/cm	$C_T^2 \times 10^{-3}$	Rf
1975	3-27-1519	4.19	0.006	9.66	, 0.004
		6.60	0.004	5.90	0.006
		7.64	0.004	1.65	0.007
		13.89	0.002	-	0.012
	3-27-1539	4.19	-0.002	10.04	-0.059
		6.60	-0.001	5.86	-0.092
		7.64	-0.001	2.58	-0.107
		13.89	-0.000	-	-0.195
	3-27-1600	4.19	-0.005	10.71	-0.032
		6.60	-0.003	3.42	-0.051
		7.64	-0.003	2.65	-0.059
		13.89	-0.001	-	-0.107
	3-27-1644	4.19	-0.002	11.25	-0.014
		6.60	-0.001	7.46	-0.023
		7.64	-0.001	3.01	-0.026
		13.89	-0.000	-	-0.048
	3-27-1656	4.19	0.0	11.31	-0.013
		6.60	0.0	5.74	-0.020
		7.64	0.0	2.08	-0.024
		13.89	0.0	-	-0.043
	3-27-2020	4.19	0.041	-	0.016
		6.60	0.026	-	0.025
		7.64	0.022	2.76	0.029
		13.89	0.012	-	0.053
	3-27-2045	4.19	0.044	5.17	0.025
		6.60	0.028	-	0.039
		7.64	0.024	0.20	0.045
		13.89	0.013	-	0.082
	3-27-2106	4.19	0.015	5.45	-0.046
		6.60	0.009	-	-0.072
		7.64	0.008	2.01	-0.083
		13.89	0.004	-	-0.151

TABLE III

April Cruise C_T^2 and Ri Results

Date Level 1

Time	$\partial\theta/\partial z$ (°C/m)	$C_T^2 \times 10^3$	Ri
4-27-1519	.135	4.439	-0.68
1529	.150	3.288	-1.15
1544	.160	2.877	-0.88
1554	.160	2.466	-0.73
1625	.160	2.634	-1.42
1635	.175	2.404	-2.04
4-28-1433	.050	5.178	-0.75
1443	.075	4.439	-0.93
1458	.050	7.398	-0.60
1517	.085	4.809	-0.80
1531	.085	5.918	-1.88
1540	.050	5.918	-20.01
1613	.075	5.548	-0.94
1618	.075	5.548	-0.90
1623	.105	4.439	-1.84
1633	.065	5.918	-1.98
1703	.035	2.877	-0.37
1720	.125	3.288	5.95
1730	.925	3.699	0.70
1740	.020	3.699	-0.47
1909	.040	2.774	1.07
1919	.040	2.959	4.45
1929	.030	3.144	5.01
4-29-1415	.025	1.099	3.34
1425	.020	3.625	0.50
2035	.040	3.625	-0.99
2050	.040	3.625	-1.48
4-30-1315	.040	4.285	-0.71
1325	.040	5.933	-1.80
1335	.050	5.273	-0.61

Data Level 2

Time	$\partial\theta/\partial z$ (°C/m)	$C_T^2 \times 10^3$	Ri
4-27-1519	.095	4.279	-1.07
1529	.105	2.445	-1.81
1544	.10	2.649	-1.38
1554	.105	2.852	-1.15
1625	.105	1.630	-2.24
1635	.11	1.936	-3.22
4-28-1433	-	-	-1.18
1443	.055	3.260	-1.46
1458	-	-	-0.95
1517	.060	4.482	-1.26
1531	.060	3.871	-2.96
1540	.035	3.871	-31.52
1613	.050	3.667	-1.48
1618	.055	4.279	-1.42
1623	.065	3.464	-2.89
1633	.015	4.279	-3.12
1703	.030	2.649	-0.58
1720	.955	3.056	9.37
1730	.001	3.260	1.11
1740	.025	3.056	-0.74
1909	.01	2.751	1.68
1919	.015	2.037	7.01
1929	.005	-	7.89
4-29-1415	.03	4.265	5.26
1425	.005	4.436	0.79
2035	.035	1.706	-1.57
2050	-	-	-2.34
4-30-1315	.020	2.730	-1.12
1325	.020	2.218	-2.83
1335	.050	3.071	-0.96

Data Level 3

Time	$\partial\theta/\partial z$ (°C/m)	$C_T^2 \times 10^3$	Ri
4-28-1340	.045	3.129	-1.69
1350	.045	2.869	-1.37
1400	.040	2.608	-1.24
1410	.040	2.869	-0.91
1423	.035	2.347	-1.21
1803	.035	0.652	-0.68
1814	.035	0.652	-0.68
1827	.015	0.782	-0.61
1836	.01	0.782	0.27
1847	.01	3.912	0.34
1858	.01	9.779	0.34
4-29-1700	.065	2.539	-7.12
1711	.08	2.537	-4.7
1722	.075	3.173	-12.6
1732	.08	3.173	-5.98
1744	.065	2.539	-5.98
4-30-1125	.05	3.491	-2.92
1137	.015	2.856	0.43
1232	.01	1.904	0.0
1242	.015	1.523	0.0
1252	.01	1.142	0.65
1302	.015	1.269	0.0

Data Level 4

Time	$\partial\theta/\partial z$ (°C/m)	$C_T^2 \times 10^3$	Ri
4-27-1519	.075	2.658	-2.24
1529	.075	1.772	-3.82
1544	.080	1.772	-2.90
1554	.085	1.772	-2.41
1625	.080	1.329	-4.71
1635	.085	1.476	-6.77
4-28-1433	.015	4.958	-2.49
1443	.035	2.953	-3.07
1458	.020	6.325	-1.99
1517	.040	4.616	-2.65
1531	.040	2.067	-6.22
1540	.025	2.658	-66.33
1613	.030	2.658	-3.11
1618	.035	2.953	-2.99
1623	.055	2.067	-6.09
1633	.045	-	-6.57
1703	.015	1.772	-1.23
1720	.075	2.067	19.71
1730	.020	2.067	2.33
1740	.010	1.772	-1.55
1909	.040	2.137	3.54
1919	.025	1.476	14.76
1929	.025	1.476	16.61
4-29-1415	.005	2.531	11.06
1425	.015	2.847	1.65
2035	.005	-	-3.29
2050	.005	-	-4.92
4-30-1315	.015	-	-2.35
1325	.015	-	-5.96
1335	.005	-	-2.03

TABLE IV

April Cruise ε Results ($\epsilon \times 10^3$)

Time	Level 1	Level 2	Level 4
4-28-1330	3.61	4.92	1.62
1339	3.97	2.90	1.66
1358	3.58	3.67	1.30
1757	4.37	4.55	1.93
1815	5.83	4.66	1.56
1833	4.68	4.95	1.88
1851	4.33	3.94	1.87
4-29-1652	12.4	4.00	6.68
1710	8.41	2.33	5.83
1728	10.4	3.04	4.17
1916	6.92	11.6	2.44
1934	5.04	1.30	1.80
2048	-	2.21	4.35
2203	17.8	3.12	1.15
2221	19.4	3.43	1.78
4-30-1013	4.87	3.43	0.84
1031	4.82	0.97	0.88
1232	7.40	2.09	1.93
1250	3.67	1.37	1.37

LIST OF REFERENCES

1. Atkinson, H. E., 1976: _Turbulent Flux Estimates from Shipboard Mean Wind and Temperature Profiles and Dissipation Rates_. M.S. Thesis, Naval Postgraduate School, Monterey, California, 66 pp.

2. Businger, J. A., J. C. Wyngaard, Y. Szumi, and E. F. Bradley, 1975: "Flux Profile Relationships in the Atmospheric Surface Layer," _J. Atmos. Sci._, 28, 184-189.

3. Cardone, V. J., 1969: "Specification of the Wind Distribution in the Marine Boundary Layer for Wave Forecasting," New York University, School of Engineering and Science, Scientific Report GSL-TR69-1, University Heights, New York, 131 pp.

4. Davidson, K. L., 1974: "Observational Results on the Influence of Stability and Wind-Wave Coupling on Momentum Transfer and Turbulent Fluctuations over Ocean Waves." _Boundary-Layer Meteorology_, vol. 6, 305-331.

5. Dyer, A. J. and B. B. Hicks, 1970: "Flux Gradient Relationships in the Constant Flux Layer," _Q. J. Roy. Meteor. Soc._, 96, 715-721.

6. Garratt, J. R., 1972: "Studies of Turbulence in the Surface Layer over Water (Lough Neagh) Part II. Production and Dissipation of Velocity and Temperature Fluctuations," _Q. J. Roy. Meteor. Soc._, 98, 642-657.

7. Hughes, M. M., 1976: _Investigation of Optically Relevant Turbulence Parameters_, M.S. Thesis, Naval Postgraduate School, Monterey, California, 63 pp.

8. Kolmogorov, A. N., 1941: "The Local Structure of Turbulence in Incompressible Viscous Fluid for very Large Reynolds Numbers," _Doklady ANSSSR_, 30, p. 301.

9. Monin, A. S. and A. M. Obukhov, 1954: "Basic Laws of Turbulent Mixing in the Ground Layer of the Atmospher," _Akademiia NAVK SSSR, Leningrad, Geofizicheskii Institut_, Trudy No. 24(151), 163-187, English Translation by Miller, J., 1959.

10. Panofsky, H. A., A. K. Blackadar, and G. G. McVehil, 1960: "The Diabatic Wind Profile," _Q. J. Roy. Meteor. Soc._, 86, 390-398.

11. Wyngaard, J. C., Y. Szumi, and S. A. Collins, 1971: "Behavior of the Refractive Index Structure Parameter near the Ground," _Jour. Opt. Soc. America_, 61, 1646-1650.

INITIAL DISTRIBUTION LIST

No. Copies

1. Defense Documentation Center   2
   Cameron Station
   Alexandria, Virginia 22314

2. Library, Code 0142   2
   Naval Postgraduate School
   Monterey, California 93940

3. Naval Oceanographic Office   1
   Library (Code 3330)
   Washington, D. C. 20373

4. Director, Naval Oceanography and   1
      Meteorology
   NSTL
   Bay St. Louis, Mississippi 39520

5. Prof. Kenneth L. Davidson, Code 63Ds   9
   Department of Meteorology
   Naval Postgraduate School
   Monterey, California 93940

6. Prof. Thomas M. Houlihan, Code 69Hm   2
   Department of Mechanical Engineering
   Naval Postgraduate School
   Monterey, California 93940

7. Dr. B. Katz, Code 213   1
   Naval Surface Weapons Center
   White Oak
   Silver Spring, Maryland 20910

8. Mr. Steve Rinard   1
   Department of Meteorology
   Naval Postgraduate School
   Monterey, California 93940

9. Prof. Dale F. Leipper, Chairman, Code 68Lr   1
   Department of Oceanography
   Naval Postgraduate School
   Monterey, California 93940

10. Captain A. Skolnick   1
    PMS 405
    Naval Sea Systems Command
    Washington, D. C. 20632

11. Lieutenant M. M. Hughes   3
    PMS 405
    Naval Sea Systems Command
    Washington, D. C.   20632

12. Lieutenant W. L. Shutt   1
    Oceanographic Unit Three
    Fleet Post Office
    San Francisco, California   96601

13. Lieutenant G. W. Karch   1
    FWC Pearl Harbor Box 113
    Fleet Post Office
    San Francisco, California   96601

14. Department of Meteorology Library   1
    Naval Postgraduate School
    Monterey, California   93940